CHAPTER 3
SACCADIC LEARNING USING VISUAL ERROR SIGNALS: SELF-MOTION VS. WORLD-MOTION AND CEREBELLAR DYNAMICS

3.1. Compensation for Initial Position in the Movement Signal

An eye can be in different positions with respect to the head before it saccades in response to a light at a fixed position on the retina. Corresponding to each different initial position, the extraocular muscles are in a different state of contraction. The same first light may thus excite the retina while the extraocular muscles are in different states of contraction. In order for a saccade to be correct in response to a first light at a fixed retinal position, it must move the eye a prescribed number of degrees no matter what initial state of muscle contraction prevails before the saccade occurs. Consequently, the total movement signal needs to take into account not only the retinal locus of a light, but also the initial state of the muscles.

Only in the case that the amount of muscle contraction is a linear function of the movement signal can this signal be independent of the initial position of the eye. This fact is illustrated in Figure 3.1. If muscle contraction is not a linear function of the movement signal, then the same movement signal can cause different amounts of contraction if the eye starts out at different initial positions. The movement signal thus cannot depend only on retinal information if the muscle plant is nonlinear, since a retinal command to move the eye ϕ degrees would move the eyes by different amounts depending upon its initial position. Since the muscle plant is nonlinear (Robinson, 1981), both retinal and initial positional information contribute to the total saccadic command.

Neither a retinally activated saccadic command nor a positionally activated saccadic command can possibly have *a priori* knowledge of the muscle plant's characteristics. Thus retinotopic and positional signals must contribute to the *conditionable* components of the total movement signal that activates the muscles. The network in Figure 2.4 must therefore be expanded to include a conditionable movement signal that is activated by a source of information about initial position (Figure 3.2).

3.2. Explicit vs. Implicit Knowledge of Initial Position

Both *explicit* and *implicit* information about initial eye position could, in principle, be used to activate conditionable movement pathways. Explicit information is computed within a network such that retinal maps and eye position maps control separate conditionable pathways that converge before the SG stage (Figure 3.2) or after the SG stage (Figure 3.3). Implicit information is illustrated by a network in which a single invariant

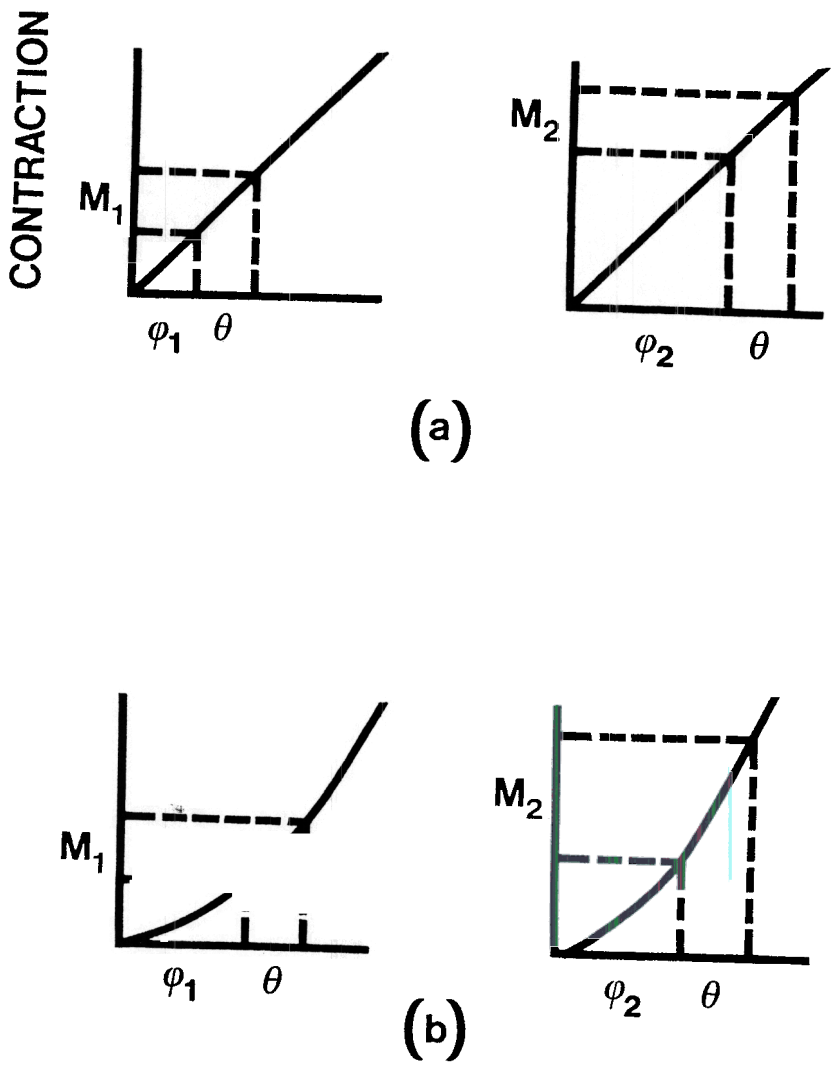

Figure 3.1. Influence of muscle plant on compensation for initial eye position: (a) In a linear plant, the amount of contraction M_1 and M_2 is the same in response to a constant retinotopic position θ given any initial eye position ϕ_1 or ϕ_2; (b) In a nonlinear plant, the amount of contraction can change as a function of initial eye position.

target position map, as described in Section 1.4, controls the conditionable pathways that project to the SG stage (Figure 3.4). A target position map contains only implicit information about eye position because each eye position inputs to many map target positions, and every map target position depends jointly upon eye position and retinal position.

In order to arrive at a complete conceptual understanding of this learning problem, we have numerically analysed how different combinations of eye position sampling maps, retinotopic sampling maps, and target position sampling maps can cooperate to correct saccadic errors due to different types of nonlinear muscle plants using either linear or nonlinear error signals. This type of parametric analysis enables us to infer how the different sampling maps to which we will be led in our subsequent analysis work together. It also shows what types of lesions within the sampling maps can automatically be compensated for by causing error signals which drive new learning within the conditionable pathways of the remaining sampling maps. In Chapter 11, this type of information will be joined to all the other learning constraints of the theory to make a global choice of model.

3.3. Characterization of Correctable Errors

In addition to classifying sampling maps that are capable of compensating for muscle plant nonlinearity, it is also necessary to characterize the error signals that are capable of correcting movement errors due to an imprecise choice of initial parameters. Three types of movement errors to which the network will adapt are:

a) movement errors due to inaccuracies of saccade length or direction; for example, undershoot and overshoot errors;

b) movement errors due to modest lesions of the eye muscles;

c) movement errors due to a contact lens on the eyeball that modestly alters the length and direction (e.g., the curvature) of visual boundaries.

Errors of type (a) can occur due to the normal course of development. Errors of type (b) can occur due to accidents. Errors of type (c) can be due either to alterations in the lens of the eye, or to experimental manipulations.

Not all experimental manipulations that alter the pattern of light reaching the retina will cause adaptation within our network model. As a simple example, no saccadic adaptation will be caused by stationary targets viewed through inverting goggles worn on the head. Such targets do not cause saccadic errors, because the real image of a stationary target is not altered by a saccade. This simple fact raises a number of questions about the types of movements that do cause errors when goggles are worn on the head, and about differences between the adaptations that occur in response to goggles vs. contact lens.

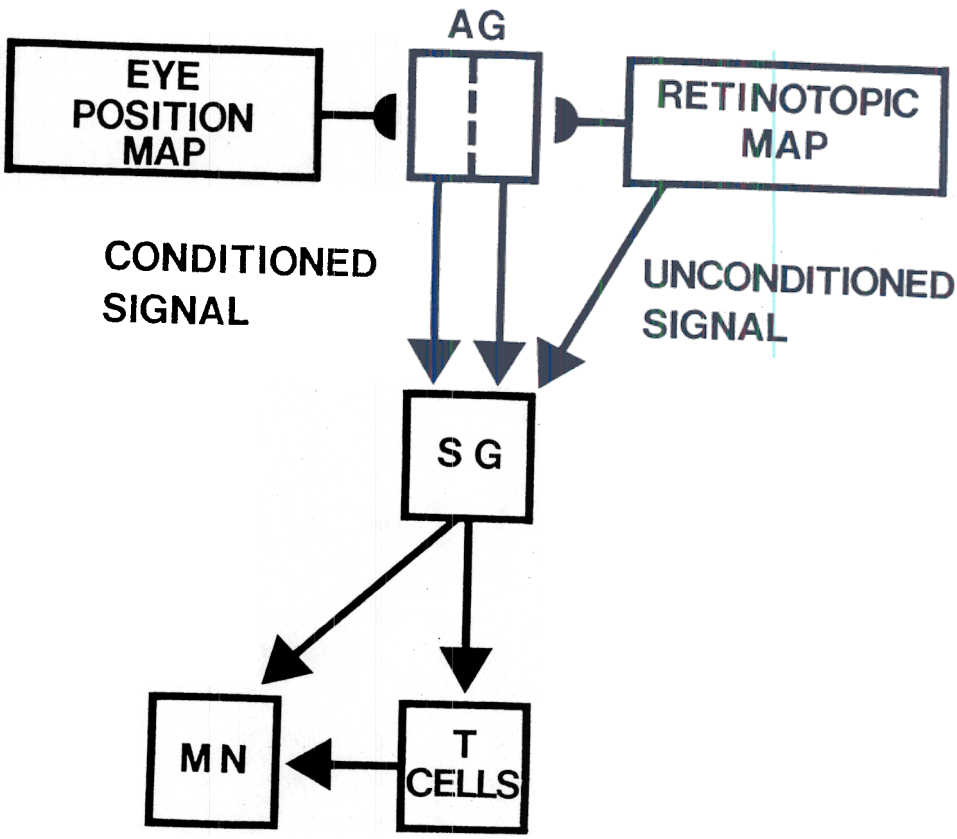

Figure 3.2. Explicit information about eye position and about retinotopic position converge at the saccade generator (SG) either via unconditioned signals or via the adaptive gain (AG) stage at which the conditioned pathways are altered by second-light error signals. T cells are tonic cells and MN cells are motoneurons.

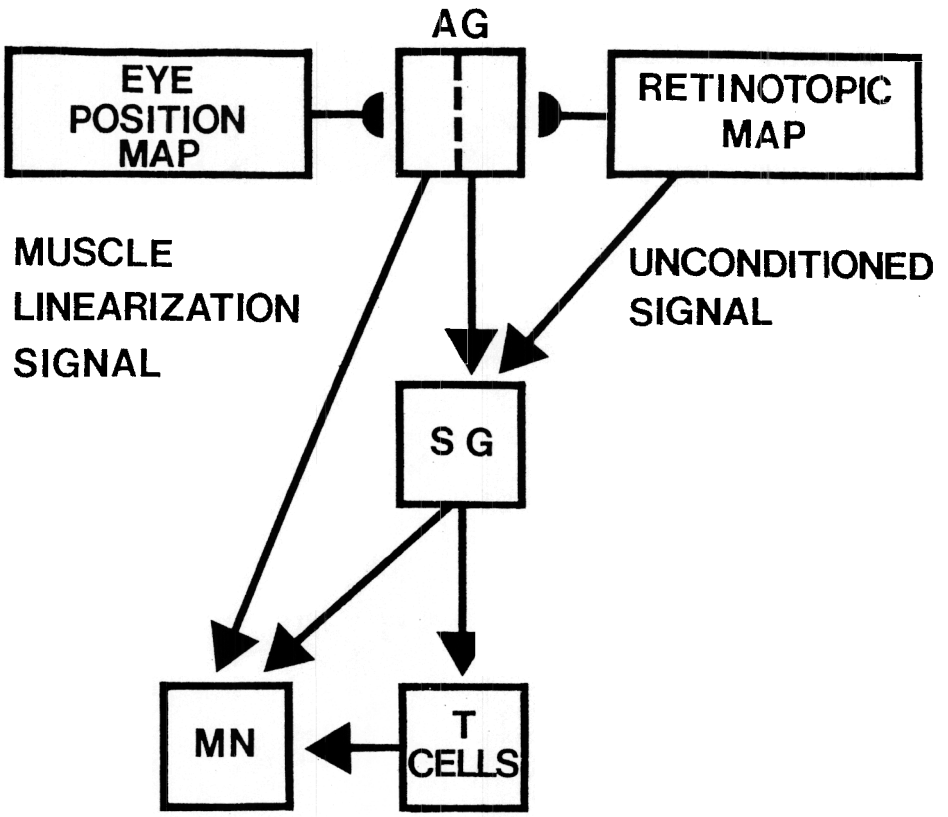

Figure 3.3. Explicit information about eye position and about retinotopic position are registered at different network stages. Retinotopic information converges at the saccade generator (SG). Eye position signals that compensate for muscle nonlinearity are registered at the motoneurons (MN). Chapters 5 and 7 refine these concepts.

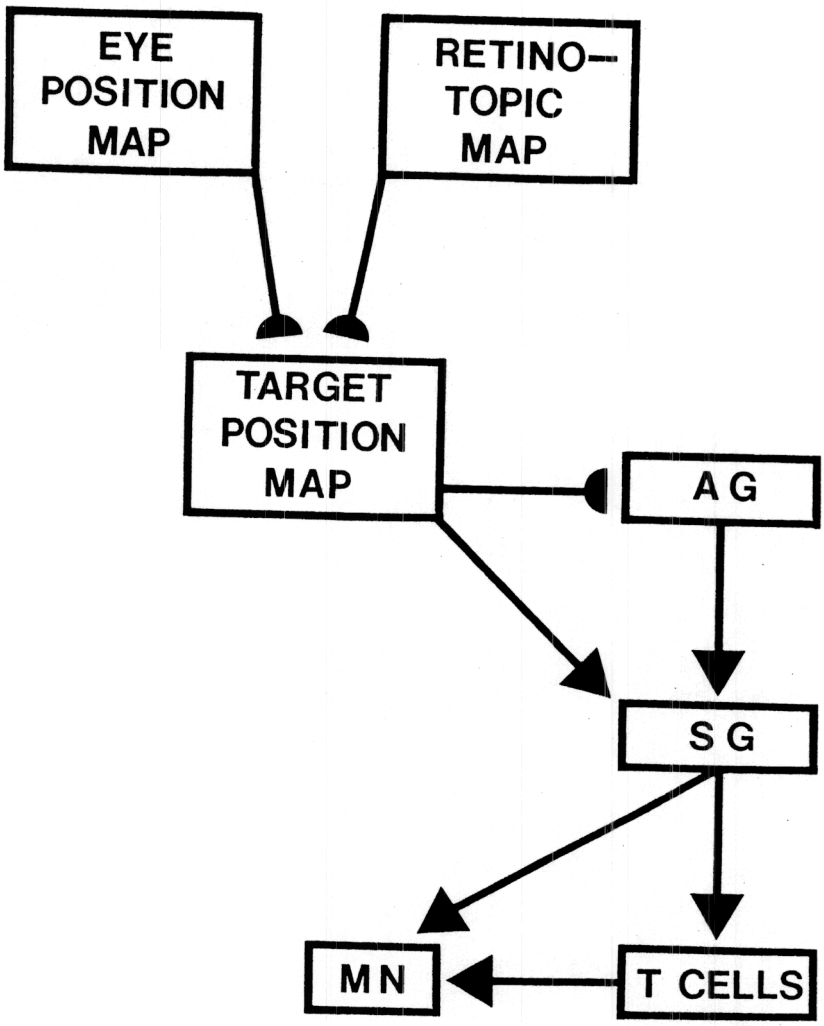

Figure 3.4. Eye position is implicitly encoded at a target position map, which is the source of both conditioned and unconditioned signals at the saccade generator (SG).

Inverting goggles do, for example, cause errors in visually-mediated reaching movements by the arm. This is because the goggles alter the expected relationship between the visual stimulus and a goal-oriented arm movement. Humans and monkeys are capable of adapting their arm movements to compensate for inverting goggles (Epstein, 1977; Welch, 1978). In pioneering experiments Stratton (1897) wore a monocular device that rotated the visual world 180 degrees for up to 8 days. He found nearly complete visuomotor adaptation when he engaged in everyday activities. Foley (1940) first studied visuomotor adaptation in monkeys. He reported that a 9-year-old rhesus monkey acquired significant adaptation after being exposed to binocular inversion for 1 week. Numerous experiments have since verified these results with finer detail and better quantification, but experiments on non-mammals show that they cannot adapt under similar conditions. For excellent reviews on many sensory-motor adaptation experiments see Epstein (1977) and Welch (1978).

Both saccadic eye movements and arm movements are goal-oriented movements that can be initiated by a visual stimulus. One might thus be tempted to conclude that saccadic eye movements can adapt to the same types of visual distortions to which goal-oriented arm movements can adapt. Inverting contact lens worn on the eye alter the visual stimuli that elicit saccades much as inverting goggles worn on the head alter the visual stimuli that elicit arm movements. Can the saccadic system adapt to an inverting contact lens?

The only direct data that we know concerning this issue yields a negative result (Smith, 1966). Our theory is compatible with this result. Our theory and the data also support the idea that adaptation can occur to contact lens which modestly distort visual curvature (Festinger, 1967; Slotnick, 1969; Taylor, 1962). What is the adaptational difference between an arm movement and a saccadic eye movement, and between an inverting contact lens and a curvature-distorting contact lens?

3.4. Self-Movement vs. World-Movement: Ballistic vs. Continuous Movement

We attribute the difference between arm and eye movement results to the different ways in which sensory-motor systems compute answers to the following question: How does the system know whether a change in visual feedback that occurs contingent upon a movement is due to self-movement with respect to a stationary world or to a movement within the world itself (Epstein, 1977)? Unless this distinction is made by an error-correcting mechanism, the mechanism cannot tell the difference between a correctly calibrated motion in a moving world and an incorrectly calibrated motion in a stationary world. An error-correcting mechanism that cannot make this distinction could persistently undo its own correct parametric calibrations in response to adventitious world motions. This destabilizing effect on the calibration of a movement system can be minimized if world-motions are rare during self-motions. The next paragraph comments upon how the rapidity of a saccade may minimize world-motions and thereby

compensate for the loss of visual information that occurs during the saccade.

In order for any error correcting mechanism to correlate movement signals and visual signals during movement, it must have access to both types of signals. Saccades differ from arm movements in that the rapidity of a saccade attenuates the registration of visual feedback during a saccadic movement. This is the familiar phenomenon of saccadic suppression (Yarbus, 1967). Due to saccadic suppression, once a given light initiates a saccade, other lights do not strongly influence the saccadic trajectory. Only lights that occur before and after the saccade can be used by the saccadic error correction mechanism. Saccades thus differ from arm movements both in their rapidity and in their approximately all-or-none reactions to light signals. We have constructed our saccadic error correction mechanism to satisfy the hypothesis that the rapidity and all-or-none nature of a saccade prevent the saccadic error mechanism from distinguishing self-motion from world-motion.

Data compatible with this hypothesis have been collected by Optican and Miles (1979). If error correction is based entirely on visual feedback after movement, the saccadic system should not be able to distinguish two different reasons why a second light might not be foveated. One reason is that an incorrect saccade is made because the system's conditionable parameters are incorrectly chosen. The other reason is that a correct saccade is made in response to correctly chosen conditionable parameters, but the light is displaced to another position during the saccade. Optican and Miles (1979) studied how monkeys saccade to lights whose position is moved to the right during saccades to the right. Although these investigators were interested in post-saccadic drift, they found that over many trials the monkeys made systematically longer saccades. Thus although the saccades of the monkeys were correctly calibrated before the experiment began, they became recalibrated by the experiment because the saccadic error correction mechanism of the monkeys could not distinguish self-motion from world-motion.

To prevent misunderstanding of this hypothesis, we emphasize what it does not imply. Compensatory processes that can distinguish self-motion from world-motion can occur in the preprocessing of visual signals before they reach the saccadic system or in the postprocessing of saccadic motor signals before they generate the final motor command. For example, imagine that preprocessing of the retinal light pattern attenuates whole-field motions of the visual field, as would be caused by self-motions in a stationary world. Such preprocessing could also amplify the reactions to relatively localized relative motions within the visual field, as would be caused by an object moving in the world. In fact, localized relative motions excite the superior colliculus with greater efficacy than whole-field motions (Frost and Nakayama, 1983), thereby tending to initiate saccades towards moving targets but not in response to self-motions alone.

Compensation for self-initiated motions can also be accomplished by postprocessing of the saccadic motor command. For example, suppose

that head movements are caused by self-motions through the world, such as walking, running, or head turning. Such a head movement can initiate a compensatory eye movement via the vestibulo-ocular reflex (VOR) to maintain the subject's gaze on a prescribed nonfoveal light (Section 3.5). Suppose, for example, that a VOR is initiated by a head movement that occurs while a saccade is being made. Then the VOR motor signal, which independently registers the head movement, can cooperate with the saccadic motor signal to generate a total movement that compensates for the self-initiated head movement (Lanman, Bizzi, and Allum, 1978; Whittington, 1980). A cooperative interaction of the VOR and the saccadic system can compensate for self-initiated head movements, even if the saccadic system by itself cannot distinguish self-motions from world-motions.

A third way to distinguish self-motion from world-motion can exist in the saccadic system as a whole without requiring that the visual error correction mechanism can make this distinction. Suppose, for example, that the eyes move with respect to a stationary light. Then the target position within an invariant target position map does not change (Section 1.4). Consequently the motor representation of this target position within the head-muscle interface (HMI) does not change (Section 1.6). No new saccadic command is therefore generated within this system due to self-motion. By contrast, suppose that a light moves with respect to the stationary eyes. Then a new target position is read into both the invariant target position map and the HMI.

The hypothesis that visual error signals due to saccades do not distinguish self-motion from world-motion implies that saccadic adaptation to inverting prisms should not occur. If saccadic adaptation to an inverting contact lens is eventually reported, then our task would be to show how a preprocessing step in the computation of the saccadic error signal distinguishes between self-motion and world-motion by using corollary discharges (Section 1.8). This preprocessed error signal would be used to alter the conditionable sampling pathways that correct saccadic errors. The data of Smith (1966) and of Optican and Miles (1979) are incompatible with the existence of such an error signal, but further experiments on this matter are needed.

Even if a negative result concerning adaptation to an inverting contact lens is confirmed, the task of explaining adaptation of visually-guided arm motions in response to inverting goggles would still remain. There is no contradiction in expecting corollary discharges to operate in this latter situation but not in response to inverting contact lens. Adaptation to inverting goggles involves intermodality (eye-arm) learning due to continuous movements. Adaptation to inverting contact lens would involve intramodality (eye-eye) learning due to ballistic movements. Thus there is a hierarchy of learning problems whose differences are reflected in the complexity of preprocessing that goes into the computation of their error signals, and in the number of sensory-motor systems that are involved. Despite these differences, all of the problems also share certain basic features in common. The next section focuses on an important shared feature of several movement systems that are capable of adapting to alterations

in expected sensory-motor relationships. After that, we begin our analysis of how the saccadic error correction mechanism of our theory works.

3.5. A Universal Adaptive Gain Control Mechanism: Saccades, VOR, Posture, and Muscle Gain

As we noted in Section 3.4, although saccades in response to a stationary visual stimulus are not rendered erroneous by inverting goggles, the eye movements that occur during the vestibulo-ocular reflex (VOR) are rendered erroneous by inverting goggles. Moreover, the VOR can adapt to these errors (Ito, 1984; Welch, 1978). Unlike ballistic saccadic movements, the VOR eye movements are sufficiently slow to permit continuous registration of visual feedback, as in the case of arm movements.

The VOR can be described as follows: a head movement triggers vestibular signals that move the eye in a compensatory way to maintain fixation of a visual target. Successful operation of this system prevents a foveated target from moving with respect to the retina of an animal as it moves with respect to its environment, say as the animal runs towards the target. An inverting goggle changes the expected relationship between head movement and the visual feedback that is caused by a VOR-induced eye movement. Thus the VOR also involves intermodality (head-eye) learning due to continuous movements.

Adaptation of eye-arm coordination and of the VOR are mentioned here to emphasize an important feature of the theory's error correction mechanisms. Adaptation to inverting goggles during the VOR seems to be a very different process from adaptation to curvature-distorting contact lens during saccades. Despite this apparent difference, the same formal network machinery can be used to control adaptive responses in both paradigms. The same formal network machinery can also be used to control adaptation to post-saccadic drift and postural maintenance of gaze (Chapter 8), as well as linearization of muscle responses to outflow signals (Chapter 5). These results support the hypothesis that a single brain region is used as a universal adaptive gain control mechanism, which we have called the *adaptive gain* (AG) *stage*. We identify the AG stage with the cerebellum.

Invoking the cerebellum as part of the adaptive saccadic mechanism is compatible with studies in which ablation of vermis and paraflocculus disrupt adaptive changes in saccadic movements (Optican and Robinson, 1980). Our adaptive gain control model also refines recent cerebellar models of VOR adaptation (Fujita, 1982a, 1982b; Ito, 1982), and sheds new light on the result of Miles, Braitman, and Dow (1980) concerning the anatomical site of VOR adaptation. In the following sections, we build up increasingly precise functional requirements concerning how the AG stage corrects saccadic errors.

3.6. Compatibility of Design Hypotheses

Two major hypotheses concerning the correction of saccadic movement errors have already been made in the preceding sections. Before imposing

additional constraints, we note that these requirements are consistent with each other, and that other possible error schemes could lead to serious internal inconsistencies.

A. *Perform and Test*

The saccadic movement system consists of many cellular components. None of these components knows the parameters governing the other components. Moreover, many of these parameters contribute to each saccadic motion. The only way that such a system can decide whether its parameters are correct or not is to test whether or not they lead to accurate foveation of light targets. Consequently, our error correction mechanism uses the position of the light on the retina after a saccade as a source of error signals.

B. *Visual Invariance during Saccades*

Thus to correct a saccade, a mechanism needs to keep track of a first light location that initiates the saccade and a second light location that is registered after the saccade. This need raises the fundamental question: How does the system know that the first and second light positions correspond to the same light source in space? How does the system know whether or not the light itself has moved during the saccade? We have hypothesized that the rapid all-or-none nature of the saccade obviates the need to distinguish world-motion from self-motion in the visual error signal.

Hypothesis (B) that no world-motion compensation occurs is compatible with hypothesis (A) that the second light is the source of light-mediated error signals. It is important to realize that not all plausible hypotheses about error signals are compatible with hypothesis (B). For example, consider a system that uses a sequence of corrective saccades leading to a correct foveation as an aggregate source of error signals. Such a system could correct saccadic errors by integrating all the corrective saccade commands into a total correct saccade command. Such a system could not, however, safely ignore world-motions that occur between successive corrective saccades. This example illustrates that a trade-off can be expected to exist in each sensory-motor system between the system's choice of error signal source and its ability to compute invariants that prevent this error source from undoing correct parameter choices.

3.7. Different Coordinates for Unconditioned and Conditioned Movement Systems

Other trade-offs exist that are capable of reconciling seemingly opposed design constraints. This section refines the conclusion of Chapter 2 that movement and error signals are processing in parallel. It shows that two different coordinate systems, working in parallel, are needed to unconditionally elicit saccades and to register the error signals that can correct these saccades.

A. *Unconditioned Movements due to Prewired Connection Gradients*

A source of unconditioned saccadic commands is needed in order to avoid an infinite regress of the following type. Unless saccades can be elicited at a developmental stage that occurs prior to saccadic learning, no saccadic errors can be generated on which to base the learning process. Since this unconditioned source of movement commands is operative prior to saccadic learning, it must be capable of working without the benefit of finely tuned learned parameters. It does not have to produce completely accurate saccades, because the later learning process will improve saccadic accuracy. On the other hand, some regularity in the transformation from retinal position to unconditioned saccadic motion is needed. For example, if a light that excites a position to the right side of the fovea elicited a movement towards the left, then the task of correcting saccadic errors would be seriously impaired.

To account for these properties of unconditioned movements, we have assumed that asymmetrically distributed pathways, or spatial gradients, are generated during an early stage of development from the retina to the eye muscles (Figure 2.1). Using these spatial gradients, a light to the right hemifield of the retina tends to move the eyes towards the right, and a light to the left hemifield of the retina tends to move the eyes towards the left. A light to an oblique retinal position tends to move the eyes in an oblique direction because the ratio of contractions in the co-contracting agonist muscles determines the net direction of movement (Grossberg, 1970; Sparks and Mays, 1981). Edwards (1980) has reported data which are compatible with such an asymmetric distribution of pathways. He writes that "the incidence of abducens-directed cells gradually increases at successively more caudal levels" of the superior colliculus (p.203).

B. *Conditioned Gain Control due to Visual Error Signals*

We will now show that the coordinates which are needed to learn error-correcting gains within the conditionable pathways are different from the spatial gradients on which unconditioned saccades are based. Thus the spatial gradients and the conditioned gains are computed by two parallel subsystems before these subsystems cooperate to read-out a total saccadic signal. We call this conditionable subsystem the adaptive gain (AG) stage (Section 3.5). Individual error lights to the AG stage must be able to correct whole muscle synergies (Section 1.11) to move the eyes closer to their targets on future performance trials. We now describe how the design of the AG stage solves this problem.

Our first observation about this problem concerns the coordinates in which first light movement signals and second light error signals are registered at the AG stage. A conditionable movement signal that is activated by a first light is registered in retinotopic coordinates, whereas an error signal that is activated by a second light must influence the gains of agonist-antagonist muscle pairs; hence is registered in motor coordinates. Both first lights and second lights arise, however, from lights on the retina. What correspondence between retinal positions and agonist-antagonist muscle pairs enables a light on the retina to be registered as a

second light in motor coordinates?

Figure 3.5a suggests an answer to this question. Figure 3.5a depicts a retinal topography that is partitioned into six motor sectors denoted by $\alpha^{\pm}$, $\beta^{\pm}$, and $\gamma^{\pm}$. Each sector corresponds to an agonist muscle (+) or its corresponding antagonist muscle (−). Each light excites the retina in a particular retinal position. As a first light, each light activates a conditionable movement pathway that retains its retinotopic coordinates. As a second light error signal, each light changes the gains of the agonist-antagonist muscle pair that corresponds to the sector in which its retinal position is contained.

C. *Opponent Processing of Visual Error Signals*

For example, suppose that the second light's retinal position falls within the sector corresponding to muscle α^+. We assume that such an error signal *increases* the conditioned gain to the agonist muscle α^+ and *decreases* the conditioned gain to the antagonist muscle α^- in response to the same first light on a later performance trial. In other words, each second light has antagonistic, or opponent, effects on the conditionable gains of its corresponding muscle pair.

To understand why this hypothesis is needed, we consider how it enables the system to correct four different types of saccadic errors.

3.8. Correcting Undershoot, Overshoot, and Skewed Saccadic Errors

Figure 3.5b considers the case of an *undershoot* error in which a first light in sector β^+ generates a second light in the same sector. To correct such an undershoot error, the second light needs to strengthen the total signal to the saccade generator (SG) of muscle β^+ and/or weaken the total signal to the SG muscle of β^-. The following considerations suggest that both a strengthening of the β^+ command and a weakening of the β^- command to the SG simultaneously occur, and help to inactivate the antagonist SG during much of a saccade.

Figure 3.5c describes an *overshoot* error in which a first light in sector β^+ generates a second light in sector β^-. After this error is corrected, a first light in sector β^+ still activates the SG of muscle β^+, but more weakly than it did before error correction. How can an error signal to sector β^- weaken the contraction of the muscle corresponding to sector β^+? The previous case of correcting an undershoot error suggests that a second light in a given sector strengthens the signal to that sector's muscle. Since muscle β^- is antagonistic to muscle β^+, both undershoot and overshoot errors can be corrected by the same mechanism if strengthening within a sector is accompanied by weakening across antagonistic sectors. The strengthening action within a sector is due to excitatory conditioning of the conditionable pathway corresponding to that muscle. The weakening action within the antagonistic sector can be accomplished in either of

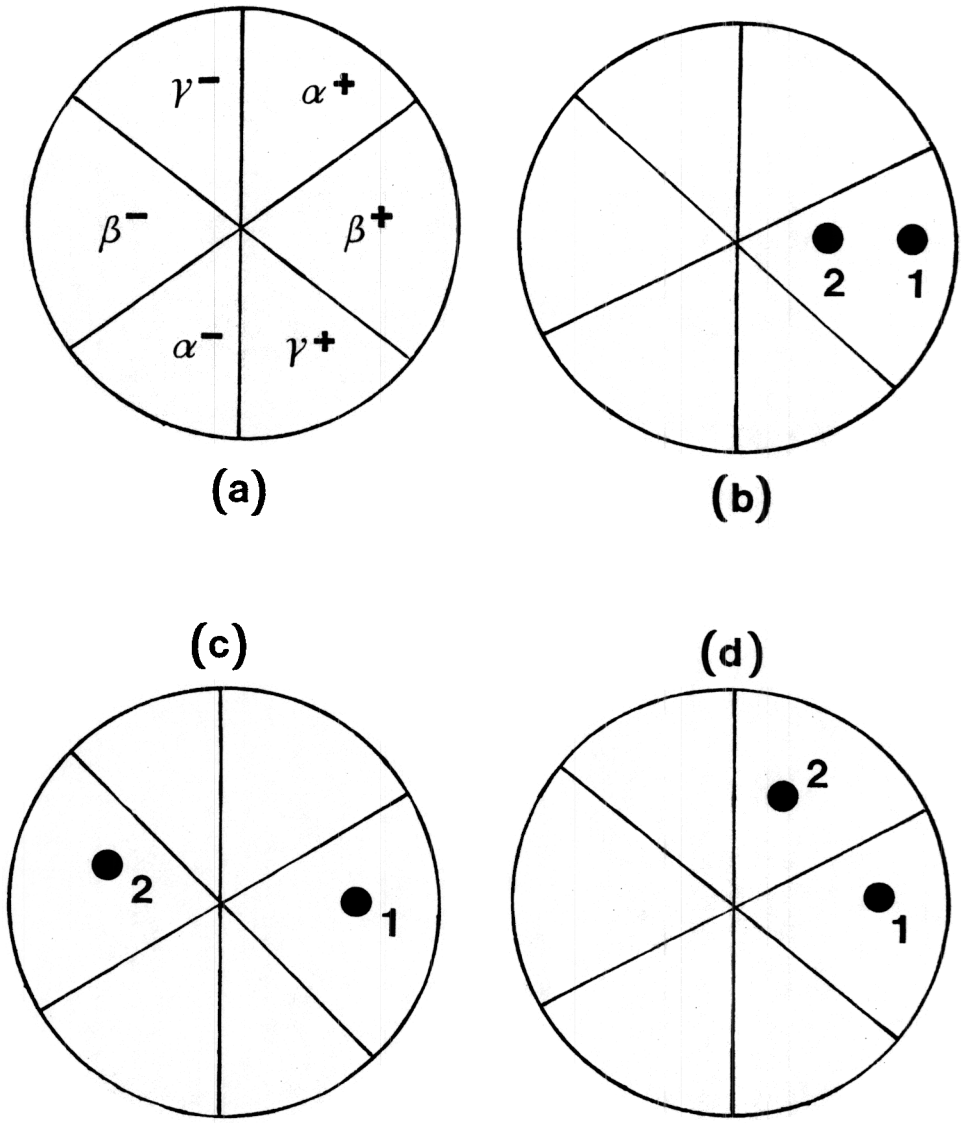

Figure 3.5. (a) Sectors corresponding to agonist muscles (α^+, β^+, γ^+) and antagonist muscles (α^-, β^-, γ^-) of one eye. In the text, the sectors represent both the retinotopic coordinates of the sampling signal sources, and the adaptive gain (AG) strips which receive error signals corresponding to the designated muscles. (b) A saccadic undershoot error. Number 1 locates the retinotopic position of the first light whereas number 2 locates the second light. (c) An overshoot error. (d) A skewed undershoot error.

two ways: by inhibitory conditioning of the conditionable pathway corresponding to the antagonist muscle (Figure 3.6a), or by inhibition of the excitatory output to the antagonist muscle (Figure 3.6b). In either case, a second light in sector β^- can weaken the total command controlled by a first light in sector β^+ via inhibitory signals from each sector to the output pathway of its antagonistic muscle. Then, when an agonist muscle contraction causes an overshoot error, the error signal corresponding to the antagonist muscle strip can weaken the conditioned gain of the agonist muscle.

The same rule easily generalizes to other types of errors. Figure 3.5d depicts a *skewed undershoot* error in which a first light in sector β^+ generates a second light in sector α^+ due to a motion of the eye downward and to the right. By the above rules, such a second light strengthens the total signal to muscle α^+ and weakens the total signal to muscle α^-, thereby tending to move the eye more upward on future performance trials to correct the movement error.

3.9. Curvature Distorting Contact Lens vs. Inverting Contact Lens

Given the above error correction mechanism, let us consider how it responds to a curvature distorting contact lens. Suppose for definiteness that the model's parameters are accurately tuned before the contact lens is put on. Let the contact lens transform radially oriented straight lines, such as a radial line in the α^+ sector of the retina, into curved lines, such as a line that crosses retinal sectors α^+, β^+, γ^+ as its retinal eccentricity increases (Figure 3.7). Radial lights placed along a radial line will then cause saccades that terminate along a curved line.

The error correcting mechanism works as follows in this situation. Consider a light that would have fallen in β^+ horizontally to the right of the fovea without the lens on, but which falls on sector γ^+ with the lens on. The eye consequently moves downwards and towards the right. Without the contact lens, the second light caused by this motion would have landed in sector α^+. Due to the contact lens, the second light lands in sector β^+. The error correcting mechanism causes the next saccade to the same first light to move in a more upwards direction to the right. By the same reasoning, the second light falls in β^+, but closer to the fovea than it did before. On successive trials, the second light falls progressively closer to the fovea, thus correcting errors due to curvature of the lens. The ability to correct such errors depends upon the property that the amount of lens distortion increases with the distance from the fovea.

By contrast, consider the effect of a contact lens that reflects the whole visual field with respect to the vertical axis. Consider a light that would have fallen in β^+ horizontally to the right of the fovea without the lens on, but which falls in β^- with the lens on. The eye consequently moves to the left. Without the contact lens on, the second light caused by this

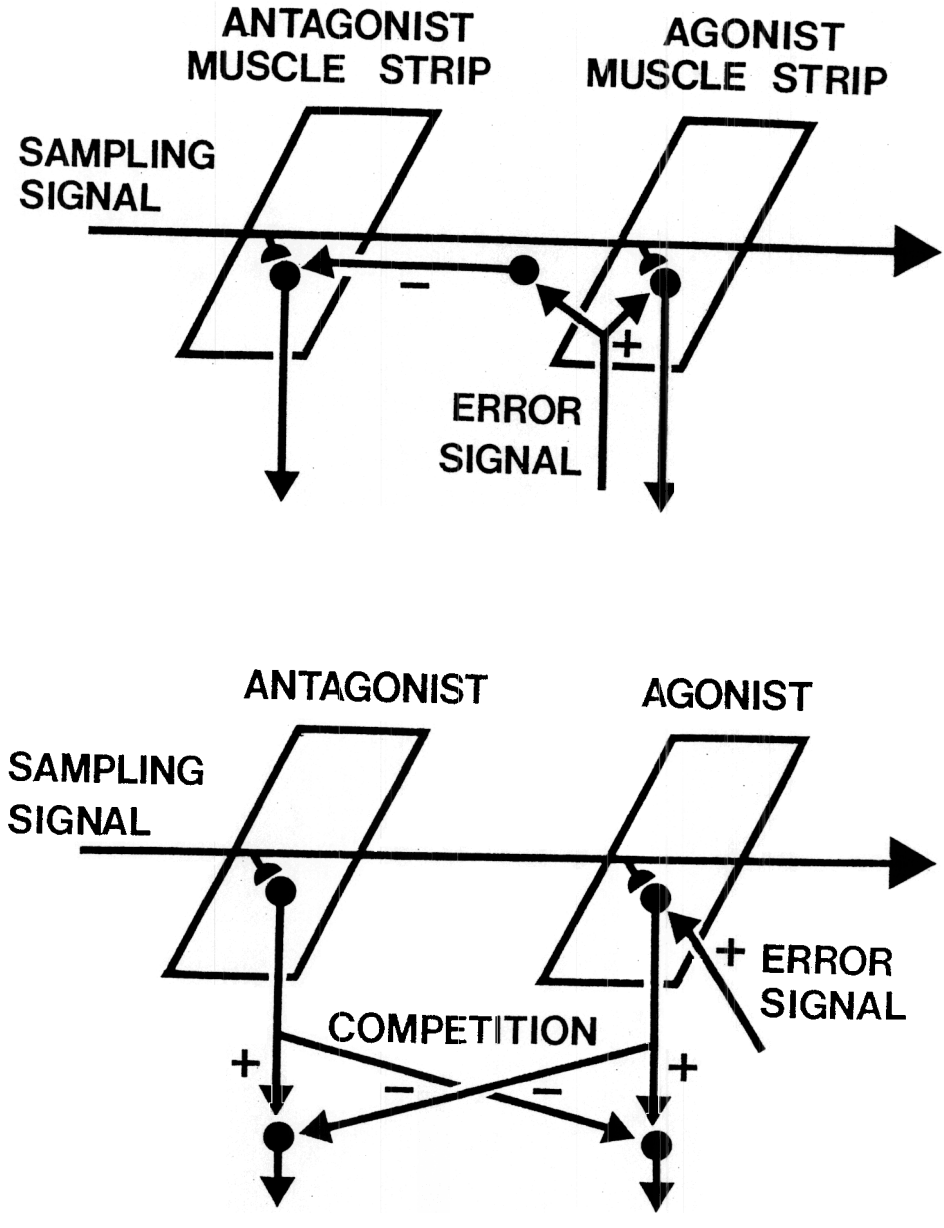

Figure 3.6. Two ways to achieve opponent conditioning of agonist-antagonist muscles: (a) An error signal increases the conditioned gain at the agonist muscle strip and decreases the conditioned gain at the antagonist muscle strip; (b) An error signal increases the conditioned gain at the agonist muscle strip. Competition between agonist and antagonist muscle strip outputs causes the decrease in the net antagonist output.

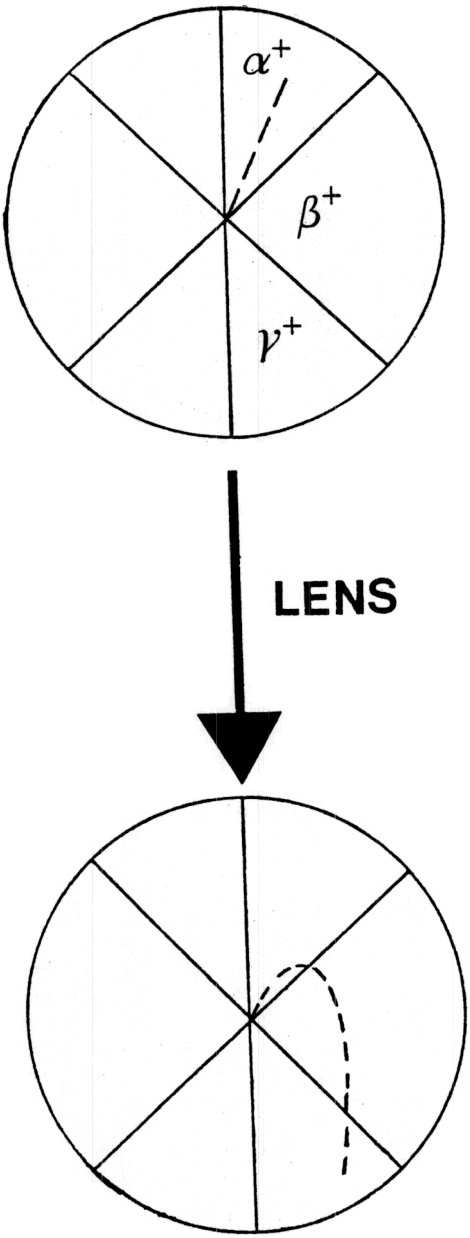

Figure 3.7. A curvature distorting contact lens which converts a linear image in sector α^+ into a curved image that bends across sectors α^+, β^+, and γ^+.

motion would have landed in sector β^+ further to the right than the first light. Due to the contact lens, the second light lands in sector β^- further to the left than the first light. The error correcting mechanism causes the next saccade to the same first light to move to the left again, but with a larger amplitude than before. By the same reasoning, the second light lands further away from the fovea than before. This tendency persists on all trials. Consequently the error is never corrected

3.10. Equal Access to Error Signals: Separate Anatomies for Unconditioned Movements and Conditioned Gain Changes

The above analysis suggests how undershoot, overshoot, skewed, and curvature distorting errors can be corrected no matter where the first light hits the retina In order for this scheme to work, a first light to *any* retinal position must give rise to conditionable pathways that can strengthen or weaken the conditioned signals to the SGs of *all* the eye muscles. Thus the asymmetric retinal-to-motor gradients that are needed to generate unconditioned saccades define the wrong kind of anatomy for saccadic error correction. These asymmetrical retinal-to-motor gradients can work even if each retinal position sends no signals whatever to the SGs of some muscles. All that is required to initiate an unconditioned saccade is a stronger pathway from each retinal position to the muscle corresponding to its sector. By contrast, correcting undershoot, overshoot, and skewed errors requires that every first light position be able to sample second lights in every sector. Expressed in another way, despite the asymmetries in the prewired retinal-to-motor spatial gradients, the mechanism whereby each first light position can adaptively sample all second light positions needs to be unbiased across second light positions. We call the property whereby each first light command can sample error signals due to all second light positions with equal ease the *equal access constraint*. We conclude that the unbiased anatomy that subserves saccadic error correction and the biased retinal-to-motor anatomy that unconditionally initiates saccades are two separate structures. We identify the error correction structure with the adaptive gain (AG) stage.

3.11. Anatomical Interpretation of the Adaptive Gain Stage: The Cerebellum

This equal access constraint suggests that the representations of all second light positions are placed symmetrically with respect to the sampling signals from any first light position. Figure 3.8 depicts the simplest realization of this concept (Grossberg, 1964, 1969a). In Figure 3.8, each first light pathway (labeled 1) gives rise to a branching conditionable pathway that is perpendicular to a series of parallel bands. Each band corresponds to one of the sectors $\alpha^{\pm}$, $\beta^{\pm}$, and $\gamma^{\pm}$. A second light in such a sector delivers an error signal to its *entire band.* Each first light can then sample any such band because its sampling pathway crosses and sends conditionable branches to all bands. The total output from such a band contributes to the conditioned gain of the corresponding muscle.

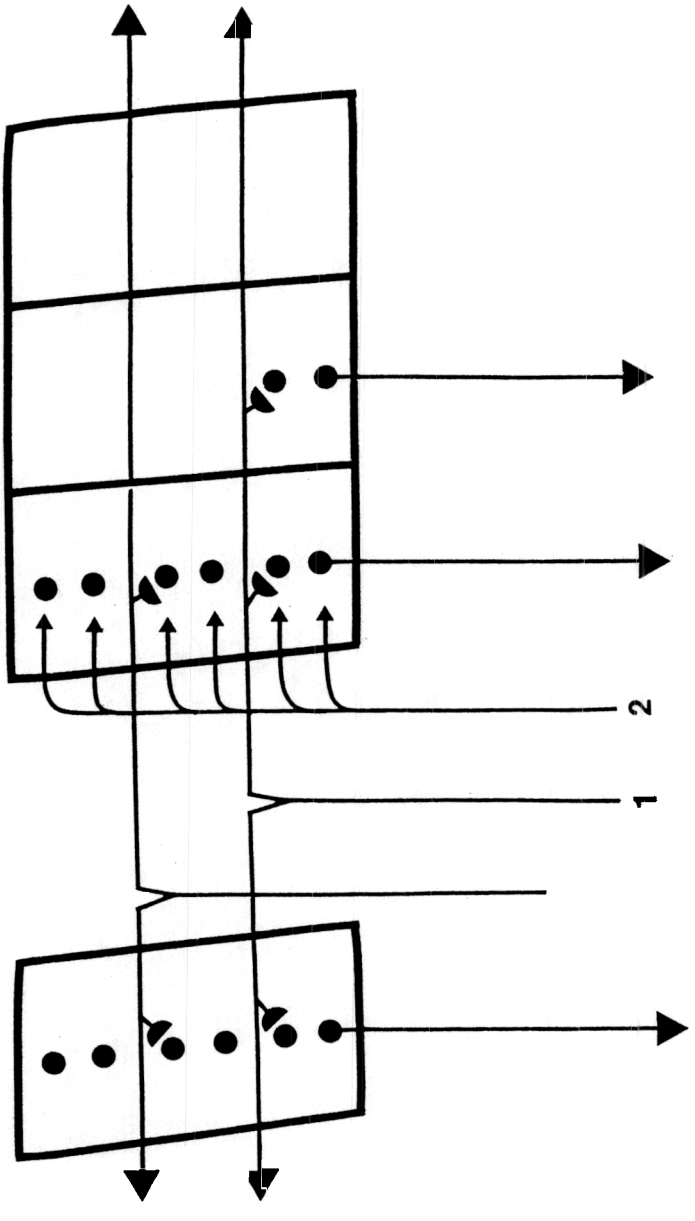

Figure 3.8. Functional diagram of the adaptive gain stage: A perpendicular arrangement of sampling signal pathways (1) and error signals (2) to motor strips enables every retinotopic coordinate to sample all motor strips and to generate output signals to all muscles.

Figure 3.8 is evocative of data on cerebellar circuitry (Eccles, 1977; Eccles, Ito, and Szentágothai, 1967; Llinás, 1969; Oscarsson, 1975) and of cerebellar models of adaptive motor control (Albus, 1971, Brindley, 1964; Fujita, 1982a, 1982b; Grossberg, 1964, 1969a, 1972a; Ito, 1974, 1980; Marr, 1969; McCormick and Thompson, 1984). In this cerebellar interpretation, the sampling pathways are realized by mossy fiber inputs that activate granule cells whose parallel fibers traverse a broad region of cerebellar cortex. The error signal pathways are realized by climbing fiber inputs that activate Purkinje cells (Figure 3.9). The synapses from active parallel fibers to activated Purkinje cells encode the adaptive changes due to the correlation between sampling signal and error signal. Our subsequent discussion will impose increasingly strong design constraints on this error correction circuit and its interaction with the asymmetric gradients of unconditioned retinal-to-motor connections.

3.12. Superposition of Sampling Map and Error Signal Map: Logarithms and Bidirectional Parallel Fibers

Some implications about the macroanatomy of the AG stage can be drawn by comparing Figures 3.5 and 3.8. By Figure 3.5, the set of all first light positions sweeps out the whole retina, as does the set of second light error signals. Thus a *map* of sampling signal sources and a *map* of error signal sources are superimposed within the AG stage. (See Section 3.16 for a discussion of examples in which the sampling signal map is not retinotopic.) The transformation of Figure 3.5a into Figure 3.8 is accomplished by mapping radial sectors into parallel strips. This property suggests that the error signal map is (approximately) logarithmic (Schwartz, 1980).

The existence of such a logarithmic map suggests, in turn, why parallel fibers are emitted by a granule cell in two opposite directions: If each retinal position activates a subset of mossy fiber terminals, then each subset must be able to activate parallel fibers capable of sampling the strips corresponding to all possible second light positions on the retina. The assumption that the parallel fibers form part of the sampling map may help to reconcile the conflicting data concerning whether parallel fibers can activate all Purkinje cells in their path. Bower and Woolston (1983) mapped the spatial organization of somato-sensory fields in the cerebellar cortex. They explored receptive field patterns in Purkinje and granule cell layers with tactile stimuli. Adjacent patches of these cell layers were found to represent widely separated body parts. They also found that Purkinje cells slightly distant from the region of granule cell layer activation occasionally responded with an increment in simple spike activity (parallel fiber excitation) for up to 100 ms. Moreover, their studies indicated that the granule cell to Purkinje cell excitation tended to be colinear with parallel fiber tracts while inhibition was slightly more widely distributed. In apparent contrast to the "parallel fiber beam hypothesis," neighboring Purkinje cells in the direction of parallel fibers often showed variable response characteristics. Only Purkinje cells for which a strong learned parallel fiber→Purkinje cells synapse exists are activated in our

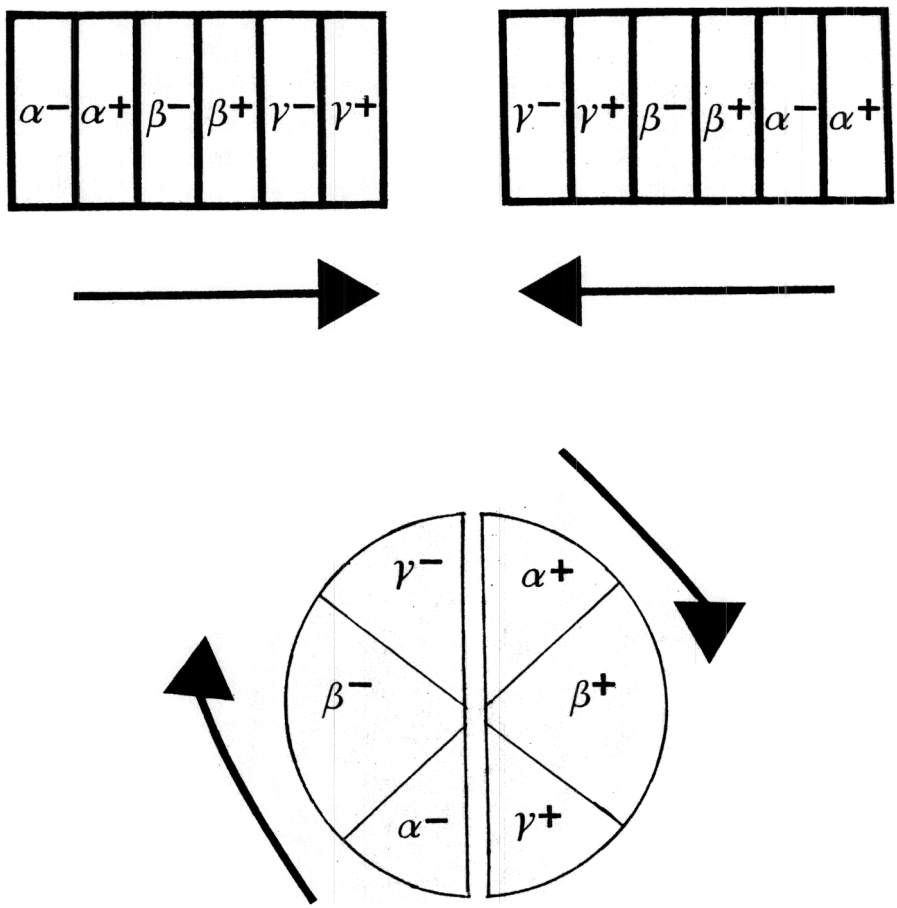

Figure 3.9. Logarithmic map from sensory sectors into motor strips: Each sensory hemifield $(\alpha^+, \beta^+, \gamma^+)$ and $(\alpha^-, \beta^-, \gamma^-)$ maps into a row of parallel motor strips. In this fractured somatotopy, the strips of agonist-antagonist pairs (α^+, α^-), (β^+, β^-), and (γ^+, γ^-) are juxtaposed, much as in the case of ocular dominance columns in the striate cortex. A pair of motor strip maps is depicted, one in each AG stage hemisphere. Outputs from all agonist-antagonist pairs compete before the net outputs perturb the saccade generator (SG). This circuit works even if only agonist muscles $(\alpha^+, \beta^+, \gamma^+)$ receive excitatory error signals in one hemifield and antagonist muscles $(\alpha^-, \beta^-, \gamma^-)$ receive excitatory error signals in the other hemifield. An excitatory error signal to the α^+ strip can weaken the net α^- output of the contiguous strip via competition of the outputs, but cannot strengthen the α^- output signal. An excitatory error signal to the α^- strip of the other hemifield can strengthen the net α^- output.

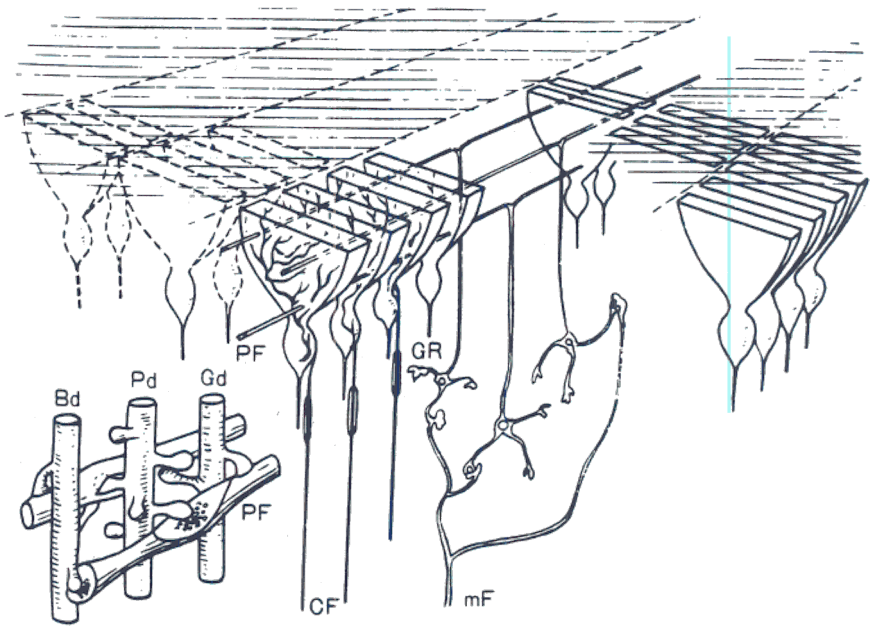

Figure 3.10. Diagram of the cerebellum showing the major cell types and interactions. The sampling signals in Figure 3.8 are assumed to be activated by mossy fibers and parallel fibers. The error signals in Figure 3.8 are assumed to be activated by climbing fibers. From Szentágothai, 1968, modified by Eccles, 1977. Reprinted with permission from **The Cerebellum and Neural Control** by Masao Ito, Raven Press, 1984.

model. Thus the receptive fields of the Purkinje cells can be regularly aligned, yet the synaptic strengths of parallel fiber contacts with these receptive fields can be much more variable.

3.13. Fractured Somatotopy and/or Bilateral Cerebellar Organization

Functional constraints on the microanatomy of the AG stage are also consistent with recent data about the cerebellum. The anatomy in Figure 3.8 can be refined by imposing the functional constraint that strengthening one conditionable pathway corresponding to a prescribed muscle weakens the net effect of the conditionable pathway corresponding to its antagonist muscle (Section 3.7). This constraint leads to the prediction that the cerebellar outputs corresponding to antagonist eye muscles vary in a push-pull, or opponent, fashion. One way to realize this property is to fracture the somatotopy of the cerebellar cortex; that is, to bring the receptive fields of agonist-antagonist muscles into a close antagonistic relationship within the cerebellar cortex, as in Figure 3.9. This type of cerebellar microanatomy has been reported by several investigators (Armstrong and Drew, 1980; Bower and Woolston, 1983; Cody and Richardson, 1979; Coffey, Goodwin-Austen, MacGillivray, and Sears, 1971; Eccles, 1973; Eccles, Faber, Murphy, Sabah, and Táboríková, 1971; Eccles, Sabah, Schmidt, and Táboríková, 1972; Saint-Cyr and Woodward, 1980). For example, a short-latency excitation of a Purkinje cell that is evoked by stimulating the ipsilateral upper lip of a rat can be suppressed by locally stimulating the contralateral upper lip (Bower and Woolston, 1983). Within our theory, such a fractured somatotopy can permit either a learned increase of agonist gain to coexist with a learned decrease of antagonist gain, or a competition to occur between output signals from the agonist and antagonist muscle strips.

Another possible way to realize an inhibitory relationship between the cerebellar pathways corresponding to antagonist eye muscle pairs is to group together the bands of all agonist muscles on one side of the cerebellum, the bands of all antagonist muscles on the other side of the cerebellum, to let each light-activated sampling pathway send parallel fibers bidirectionally across the midline of the cerebellum to sample all these bands, and to let the outputs of antagonistic bands compete across the midline before the net output influences the corresponding SGs.

A combination of these two designs is also possible. In this anatomy, agonist muscles of one eye are brought into a close antagonistic relationship in the cerebellar cortex. Thus strengthening the gain of one agonist muscle via an error signal weakens the gain of the other agonist muscles, thereby shifting the vector direction of agonist contraction in that eye. Somatotopy is fractured by bringing together the agonist representations of corresponding muscles in the two eyes, and letting the error signals that strengthen an agonist muscle command in one eye also strengthen the agonist command of the corresponding muscle in the other eye. At least partial adaptive yoking of the two eyes is hereby achieved. All agonists

are represented on one side of the cerebellar cortex, all antagonists are represented on the other side of the cerebellar cortex, and the outputs of agonist-antagonist bands compete across the midline before the net output influences the SGs. We mention all of these anatomical possibilities because, even if one of them is supported in one species, we must still be prepared to understand different versions of this mechanism that may be used by other species.

Eckmiller and Westheimer (1983) have reported data that are consistent with the last two anatomies. These authors show that ablation of the cerebellar cortex on one side in monkeys causes deficits of eye movements on the lesioned side. If future anatomical studies show that fractured somatotopy occurs in the cerebellar vermis, then the third anatomical possibility is favored.

Ebner and Bloedel (1981) have reported cerebellar data that are compatible with the third possibility, albeit not in a cerebellar circuit that subserves saccadic control. These authors described the correlations of spontaneous climbing fiber inputs with mossy fiber activations due to flexions of the forepaw. They found that if a mossy fiber tended to enhance activity of a Purkinje cell before being paired with climbing fiber activity, then this enhancing effect was amplified after termination of climbing fiber activity. They also found that if a mossy fiber tended to depress activity of a Purkinje cell before being paired with climbing fiber activity, then this depressive effect was amplified after termination of climbing fiber activity. Gilbert and Thach (1977) also described compatible cerebellar data. They showed that if a known extensor load is increased to a novel load level, then an increase in climbing fiber activity is caused that leads to a decrease in later Purkinje cell activity in response to mossy fiber inputs. The climbing fiber input frequency to a known flexor load did not change, but the Purkinje cell activity caused by mossy fiber input decreased. These results during the known flexor motion are compatible with the existence of an agonist-antagonist fractured somatotopy, and also suggest that learning can cause a decrease in synaptic strength. The ratio of gains across agonist-antagonist pathways can also be changed by such a learning mechanism.

As part of their studies of the VOR, Ito and his colleagues (Ito, 1982; Ito, Sakurai, and Tongroach, 1982) have also reported data indicating that climbing fiber inputs that are correlated with mossy fiber activity can depress the responsiveness of target Purkinje cells to later mossy fiber inputs. This depression was caused by conjunctive stimulation of a vestibular nerve (mossy fiber) and of the inferior olive (climbing fiber). Llinás and Wolfe (1977) have recorded from saccade related Purkinje cells in the cerebellar vermis. They found some Purkinje cells that fired at a rate inversely proportional to the amplitude of concurrent saccadic eye movements. They attributed this Purkinje cell activity to "the highly stereotyped spike burst characteristics of climbing fiber induced activity" (p.4). Such an effect could be produced by changes in the ratio of agonist-antagonist activation recorded at the antagonist motor strip of the saccadic command.

Such cerebellar results are consistent with our model, but do not unequivocally support or reject it, primarily because these data do not directly measure cerebellar effects on antagonistic muscle pairs as a result of learning. The functional constraints that our theory imposes on cerebellar design are consistent with many evolutionary variations. If our theory is correct, however, then all of these variations must embody a form of agonist-antagonist opponency whose balance can be regulated by learning.

3.14. More Constraints on Cerebellar Learning

Further constraints on the saccadic learning mechanisms will now be derived and shown to be realizable by several related mechanisms. The physiological data do not yet seem to decide between these alternatives either. Part of the ensuing discussion applies only to the problem of saccadic error correction. For example, the saccadic learning problem under consideration is a case of temporally discrete sampling wherein both sampling and error signals can be activated by the same modality, namely vision. By contrast, the VOR describes a continuous sampling problem wherein the sampling signal is vestibular and the error signal is visual. Differences therefore exist in the types of sampling signals and sampled signals that are used for saccadic vs. VOR adaptation. Part of the discussion nevertheless has general implications for cerebellar design. Although each learning circuit, whether mediating saccades or VORs, may preprocess its inputs in different ways, we believe that the same internal cerebellar machinery is used in all cases.

The following hypotheses about cerebellar learning will be explored below:

A. The dual action of each light.

B. The incremental effect of error signals on performance.

C. The attenuation of error signals by prior learning trials.

3.15. Dual Action, Incremental Learning, and Error Signal Attenuation

By the dual action of each light, we mean that each light is a source of an error signal for correcting a previous saccade, as well as a source of a movement command for the next saccade By the incremental effect of error signals on performance, we mean that the effect of error signals is to progressively improve the accuracy of saccades. In particular, as learning progressively increases the conditioned gain of an agonist muscle, it progressively decreases the conditioned gain of its antagonist muscle. This opponent learning process biases which of the saccade generators corresponding to the two muscles will be activated. By the attenuation of error signals due to prior learning trials, we mean that saccadic error correction tends to undermine its own source of error signals by causing more accurate saccades. This last property is the main justification for calling the second light a source of error signals. This property implies

that the size of the error signal generated by a second light decreases as the second light approaches the fovea.

These three properties imply further constraints upon the microscopic design of the AG stage. The main constraints arise from a consideration of how sampling signals and error signals are allowed to overlap in network space and time in order to realize these three functional properties.

The dual action of each light constrains the possible onset times and durations of sampling signals and error signals. To see why this is so, suppose that the eyes make a sequence of inaccurate saccades in response to a single unmoving light in the outside world. These saccadic movements generate a series of lights on the retina. Denote the sampling signal due to the ith light in such a saccadic sequence by S_i and its error signal by E_i, $i = 1, 2, \ldots$. Several possible cases may arise, and our goal is to indicate which cases are consistent with functional requirements. If inconsistent cases are found *in vivo*, then our model of cerebellar learning needs correction.

Case 1: Suppose that the onset time of E_i precedes that of S_i and that E_i terminates before S_i begins (Figure 3.11a). Since S_{i-1} must sample E_i, the offset time of S_{i-1} is later than the onset time of E_i. In this situation, E_i can alter the effect of S_{i-1} on future performance without altering the effect of S_i on future performance, even though both S_i and E_i are elicited by the same light.

Case 2: Suppose that the onset time of E_i is subsequent to the onset time of S_i (Figure 3.11b). Since S_{i-1} must be able to sample E_i, S_{i-1} is still active in SSTM at the onset time of S_i. The timing configuration in Figure 3.10b can create the following difficulty.

The effect of an error signal such as E_i on the sampling signal S_{i-1} of a prior light is to progressively improve the accuracy of the saccade that corresponds to S_{i-1}. Thus after sufficiently many learning trials take place, S_{i-1} will read-out conditioned signals leading to accurate foveations which generate zero error signals. In order for E_i's to correct an S_{i-1} in this way, the effect of successive E_i's on the conditionable pathway sampled by S_{i-1} must be incremental, so that each successive saccade foveates better in response to the same first light. When this incremental learning effect ultimately causes accurate foveations, no further error signals are registered until parameter changes elsewhere in the system cause fixation errors anew.

Given these learning properties, an S_i that overlaps its own E_i on every trial, as in Figure 3.11b, can create a serious learning anomaly. If a given nonfoveal light increments its S_i-activated sampling pathway with its own nonzero E_i on every saccadic trial, then the error signal never terminates even if the saccade becomes more accurate. Unless precautions are taken, every saccade will eventually overshoot due to the persistent action of its own error signal. Can this problem be prevented if the timing relationships of Figure 3.11b prevail?

This problem cannot be escaped just by claiming that S_i is insensitive to E_i because S_i's onset time precedes that of E_i. Such a sensitivity-

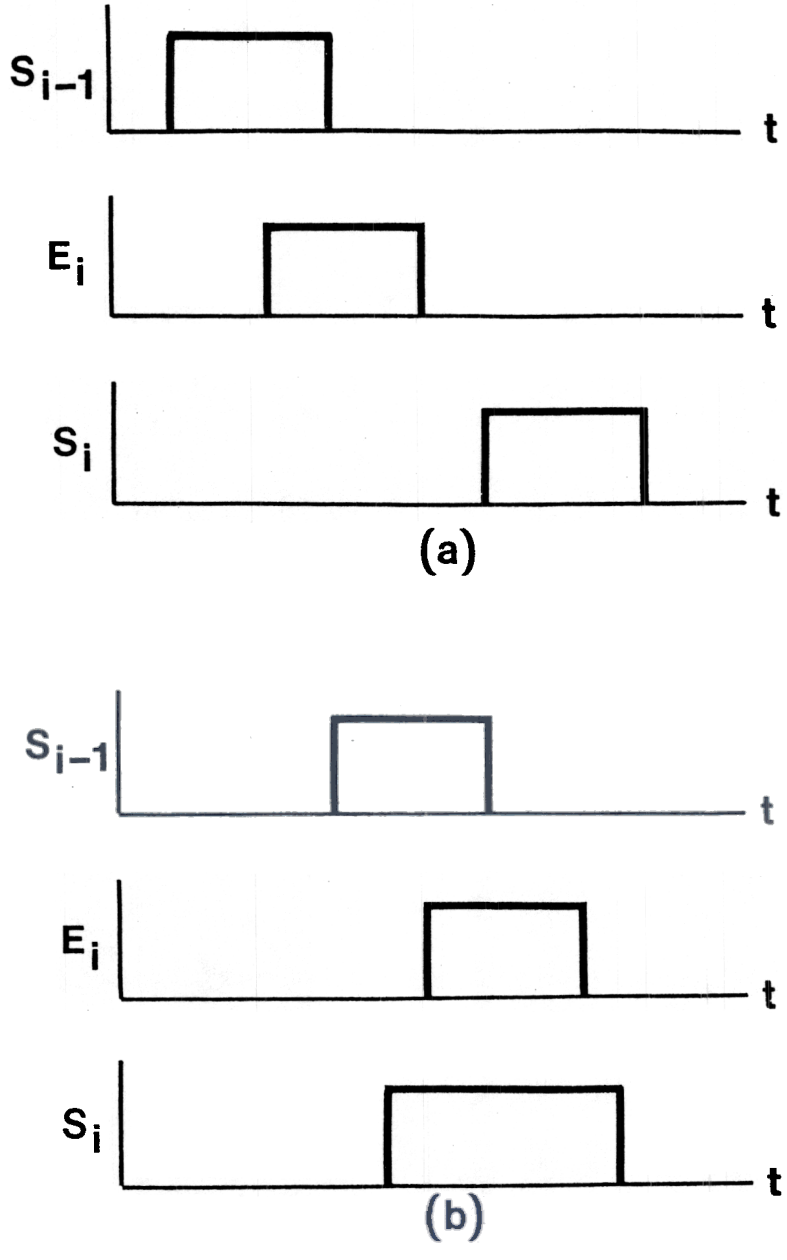

Figure 3.11. Two possible configurations of sampling signals and error signals: S_j is the sampling signal and E_j is the error signal on the jth trial, plotted through time.

timing argument fails because S_{i-1} must be sensitive to E_i even though the onset time of S_{i-1} precedes that of S_i. If S_i were already insensitive to E_i when E_i occurred, then surely S_{i-1} would also be insensitive, thereby preventing any saccadic learning whatsoever from occurring.

This self-sampling problem can be overcome if a preprocessing stage exists at which both the sampling map and the error map are topographically superimposed. Suppose at this stage that the source of sampling signals due to a given light topographically inhibits the source of error signals due to the same light before the error signals reach the AG stage. Then no S_i could sample its own E_i, although any active $S_{i-1} \neq S_i$ could sample E_i.

Cases 1 and 2 show that two different timing rules can, in principle, govern cerebellar learning if these rules are joined to suitable topographic restrictions on self-sampling of error signals.

3.16. Numerical Studies of Adaptive Foveation due to Cerebellar Gain Changes: Learned Compensation for System Nonlinearities

We have numerically analyzed the formal learning capabilities of several types of AG stage models to achieve a quantitative understanding of the AG stage concept. We have sought the type of understanding that can meet the challenge of species-specific variations of several conceivable types. We have paid particular attention to the issue of muscle nonlinearity. To this end, we have carried out computer simulations wherein different combinations of eye position sampling maps, retinotopic sampling maps, and target position sampling maps are used with two varieties of agonist-antagonist competitive interactions to learn accurate foveations using different types of nonlinear muscle plants and error signals. This type of parametric analysis provides a conceptual understanding that transcends the limitations of any single model.

In this spirit, we have systematically analyzed how thirty-six related models learn visually reactive (non-predictive) sequences of saccades, and have studied the stability of learning in each model given several numerical choices of important parameters. Eighteen of the models use a learning rule that instantiates a fractured cerebellar somatotopy and eighteen of the models use a learning rule that instantiates a bilateral cerebellar organization (Section 3.7). Both types of anatomy use an incremental learning rule (Section 3.15). Within each of these learning types, six of the models use a linear error signal and twelve use two different nonlinear error signals. All the error signal functions increase with the distance of a second light from the fovea. The different error signal functions embody different spatial gradient rules that transform a second light in retinotopic coordinates into an error signal in motor coordinates. The six model choices corresponding to each choice of error signal embody different strategies for compensating for initial eye position. These strategies will be described in the following paragraphs.

In all cases, saccades converge to the correct target position, on the average, with increasing numbers of learning trials. However, the errors fluctuate around the correct target position in a manner that depends in a systematic way on the design of the system. Given a nonlinear muscle, a significant damping of errors occurs only if initial position is taken into account in the learning rule. The following empirical rule has been derived from our studies of these thirty-six models.

The Nonlinear Dimension Rule: An extra degree of freedom in the sampling maps is needed to compensate for each nonlinearity in the muscle response.

The remainder of this section describes the results of these computer simulations in an intuitive language. Section 3.18 defines the learning models mathematically.

A. *Purely Retinotopic Sampling*

To see that compensating for a nonlinear muscle plant is a real problem, consider Figure 3.12. In Figure 3.12A, only a retinotopic sampling map can be conditioned by error signals. Figure 3.12A shows that, although saccades become more accurate on the average due to learning, the mean error rate never becomes smaller than approximately $\pm 6.7\%$ of the total visual field. The negative result holds even if the error function increases linearly with distance of the second light from the fovea, and if the relationship between muscle contraction and motion of the light on the retina is equal and opposite.

The cause of this learning difficulty is the nonlinear relationship between the total saccadic signal and the amount of muscle contraction. In the system of Figure 3.12A, this nonlinearity is a slower-than-linear one: The amount of contraction is proportional to the saccadic command at small values of the command, and gradually begins to decrease, or to saturate, at larger values of the command. In this example, a half-maximal muscle signal causes a 4/5-maximal muscle contraction. Thus the nonlinearity has a significant effect on system performance.

Figure 3.12B shows that the nonlinear muscle function is the cause of this difficulty. When a linear muscle function is used, essentially perfect learning occurs. This occurs even though a demanding rule is imposed governing the amount of muscle contraction and the corresponding motion of the light on the retina: an increment of ΔL in muscle contraction is assumed to cause a change $-2\Delta L$ in the position of the light on the retina.

In order to learn well using a nonlinear muscle plant, the learning system needs somehow to compensate for the different contractions that are caused by fixed movement signals when the muscle starts out in different initial positions. A retinotopic sampling map contains no information whatsoever about initial position. The remaining simulations include information about initial position in several different forms. In the computer studies that are summarized below, we considered a mean error rate to be unacceptable unless it was less than about 4 percent of the visual field. This approximates the accuracy of human saccades (Weber and Daroff, 1972).

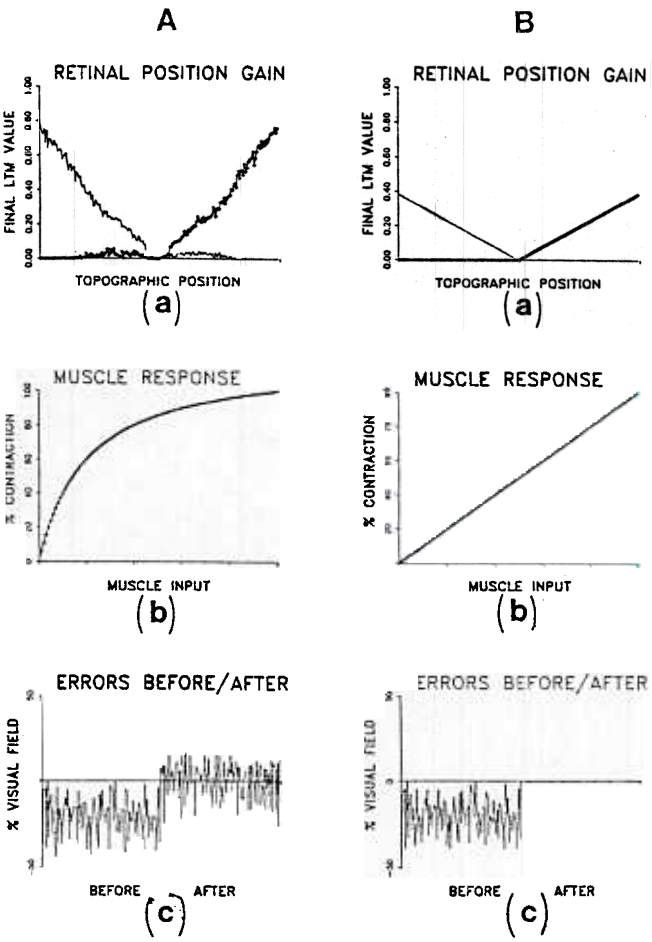

Figure 3.12. Computer simulation of saccadic error correction model with sampling from retinal position map using a linear learning function $L(w) = \epsilon w$: (A) Slower-than-Linear Muscle Function: The following parameters were used in the simulation: $m = 1$, $\alpha = .2$, $\gamma = 1$, $\delta = 1$, $\epsilon = .01$, and $n = 100,000$. (a) Topographic distribution of LTM trace values after learning. Bold curve indicates values in the right adaptive gain (AG) stage hemifield. Thin curve indicates values in the left AG stage hemifield. (b) Muscle response function used in the simulation. (c) Errors in 100 trials before learning begins and 100 trials after learning ends. Negative values correspond to undershoots and positive values correspond to overshoots. Learning was poor. (B) Linear Muscle Function: The following parameters were used: $\gamma = 2$, $\delta = 1$, $\epsilon = .01$, and $n = 100,000$. Learning was perfect.

B. *Invariant Target Position Map*

One way to take the initial eye position into account without increasing the total number of long-term memory (LTM) traces in the sampling maps is to let a single LTM trace multiply a composite signal that is the sum of two signals. Let one signal code a retinotopic light position, the other signal code an initial eye position, and the two signals add to influence a single LTM trace only if their sum represents a fixed target position. A different LTM trace exists corresponding to each target position that is computed within the spatial resolution of the network. Such a sampling map is called an invariant target position map because a single LTM trace corresponds to each target position independent of how that position is synthesized from its component signals (Section 1.4).

In this system, a single LTM trace must compensate for all the initial eye positions that can correspond to a fixed target position. Each of these initial eye positions corresponds to a different part of the nonlinear muscle function. Despite this fact, a significant reduction in the mean error rate occurs compared to the case of purely retinotopic sampling. Figure 3.13 depicts a simulation in which the mean error rate eventually becomes 1.8% of the visual field. Thus if a single sampling map implicitly embodies two degrees of freedom (one retinotopic position plus one initial eye position), then excellent learning occurs (Section 3.2).

C. *Invariant Target Position Map Plus Retinotopic Map*

Increasing the number of adaptive degrees of freedom causes a further improvement in error rate, even if no more LTM traces correspond to initial eye position information *per se*. These additional degrees of freedom enable part of the burden of adaptation to be absorbed by a different sampling map. In Figure 3.14A, both an invariant target position map and a retinotopic map separately send sampling signals to the AG stage. Each of these maps undergoes independent learning within the AG stage. The two sampling maps then add their conditioned movement signals to unconditioned movement signals at the SG. The LTM traces of the independent retinotopic map and invariant target position map embody three degrees of freedom. The retinotopic map explicitly embodies one degree of freedom and the invariant target position map implicitly embodies two degrees of freedom. In these simulations, a mean error rate of 1.5% of the visual field was attained using a nonlinear S-shaped muscle function. Thus if three degrees of freedom are used and at least one degree of freedom incorporates initial eye position signals, then excellent learning takes place. This is true even if the learning function is nonlinear; for example, if error signals grow as a cubic function of error size.

D. *Retinotopic Map Plus Eye Position Map*

Better learning than with purely retinotopic sampling (Figure 3.12A) occurs using two degrees of freedom in which the first map is a retinotopic map and the second map is a map of initial eye position. In these simulations, the network takes into account the target position of the eye (initial position plus retinal light position), but does not compute a map whose individual cells represent target position (Figure 3.14B). In these

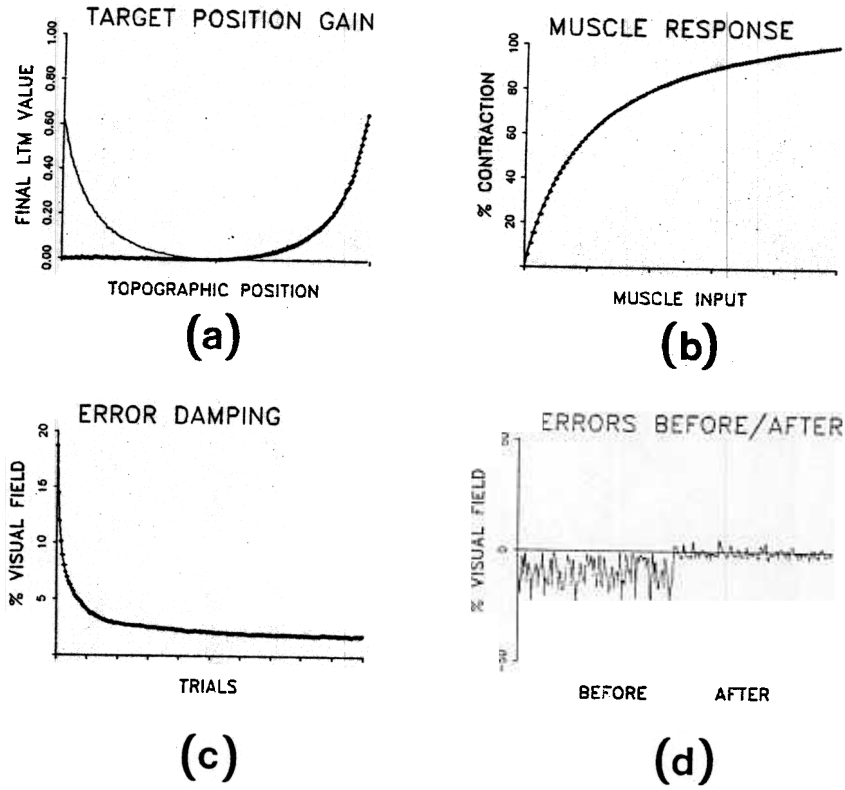

Figure 3.13. Computer simulation of saccadic error correction model with sampling from an invariant target postion map using a slower-than-linear muscle function and a linear learning function. The following parameters were used in the simulation: $m = 1$, $\alpha = .2$, $\gamma = 1$, $\delta = 1$, $\epsilon = .01$, and $n = 100{,}000$. (a) Topographic distribution of LTM trace values after learning. Bold curve indicates values in the right adaptive gain (AG) stage hemifield. Thin curve indicates values in the left AG stage hemifield. (b) Slower-than-linear muscle response function used in the simulation. (c) Error damping over 100,000 trials. Error damping value D_n at trial n approximates the average error via the equation $D_{n+1} = (999D_n + \mid E_n \mid)/1000$, where $D_0 = 25$. (d) Errors in 100 trials before learning begins and 100 trials after learning ends. Negative values correspond to undershoots and positve values correspond to overshoots.

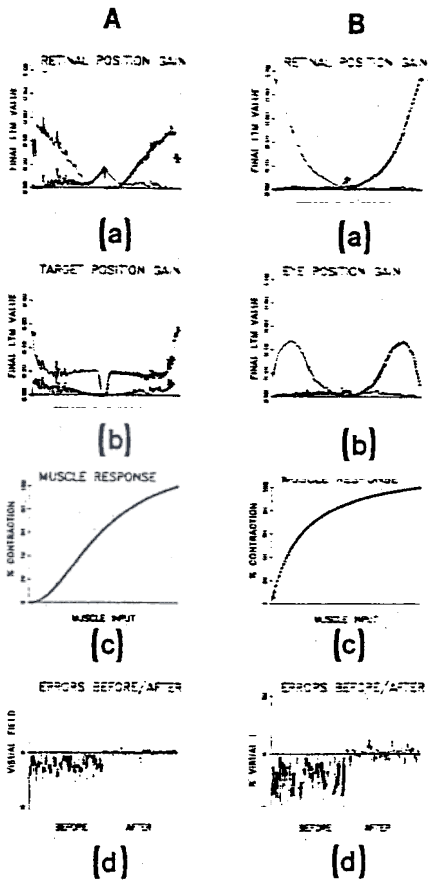

Figure 3.14. Computer simulation of saccadic error correction model with two sampling signal maps. (A) Sampling from an invariant target position map and a retinal position map using an S-shaped muscle function and a cubic learning function. The following parameters were used in the simulation: $m = 2$, $\alpha = .5$, $\gamma = 1$, $\delta = 1$, $\epsilon = 1$, and $n = 1{,}000{,}000$. (a) and (b) Topographic distribution of LTM trace values after learning. Bold curves indicate values in the right adaptive gain (AG) hemifields while the thin curves indicate values in the left AG hemifields. (c) Sigmoid muscle response characteristic used in the simulation. (d) Errors in 100 trials before learning begins and 100 trials after learning ends. Negative values correspond to undershoots and positive values correspond to overshoots. (B) Sampling from a retinal position map and an initial eye position map using a slower-than-linear muscle function and a linear learning function. The following parameters were used in the simulation: $m = 1$, $\alpha = .2$, $\gamma = 1$, $\delta = 1$, $\epsilon = .01$, and $n = 1{,}000{,}000$.

simulations, a mean error rate of 3.5% of the visual field was attained using a nonlinear slower-than-linear muscle function. Note that, although both Figures 3.14A and 3.14B use two sampling maps, their final error rates and spatial distributions of LTM traces are different due to their different sampling maps and the different nonlinear muscle plants to which they are adapting. In other words, different sampling maps automatically learn different LTM patterns to compensate for the initial position errors that are caused by different nonlinear muscle functions.

E. *Noninvariant Target Position Map*

Two degrees of freedom can also be realized by allowing every possible pair of retinotopic positions and initial eye positions, up to some finite spatial resolution, to have its own sampling pathway and LTM trace. Figure 3.15 shows that this model can achieve arbitrarily good mean error rates. Because each unique pair of positions has its own LTM trace, learning by this model is very stable. The model has the disadvantage that a given LTM trace will not be tuned until its unique pair of positions is activated on learning trials. By contrast, when an invariant target position map is used, learning occurs at a retinotopic or initial eye position whenever this position is a component of any target position. Thus there exists a tradeoff between convergence rate, stability, and the number of independent sampling sources. The expected interval between successive learning increments at each LTM trace of a noninvariant target position map can be decreased by expanding the receptive fields of positions in the sampling map. Then positions near to a fixed position can induce some learning at that position. The LTM traces then attain limiting values that are averages of the gains appropriate to nearby map positions. Given sufficiently symmetric and localized receptive fields, these average LTM values approximate the values that occur without any receptive field spread, but at a faster rate.

F. *Retinotopic Map Plus Initial Eye Position Map Plus Invariant Target Position Map*

If three independent sampling maps send sampling signals to the AG stage, then learning is again very accurate and stable. Figure 3.16 depicts an example in which a muscle contraction of ΔL causes a change of $-2\Delta L$ in the retinal position of the light. Despite this distortion, the system quickly achieves error rates of .3% of the visual field.

3.17. Shared Processing Load and Recovery from Lesions

Inspection of Figures 3.12–3.16 shows that the spatial maps of LTM traces that arise due to learning in different models need not be the same. For example, the retinotopic LTM map or the invariant target position LTM map may differ due to the existence of other sampling maps in the network. These results illustrate that the adaptive behavior of each region of the network is influenced by the design of the network as a whole. Each region automatically assumes a different share of the processing load depending upon how many other regions exist to share this load. This type of insight helps to explain experiments wherein behavioral losses right after

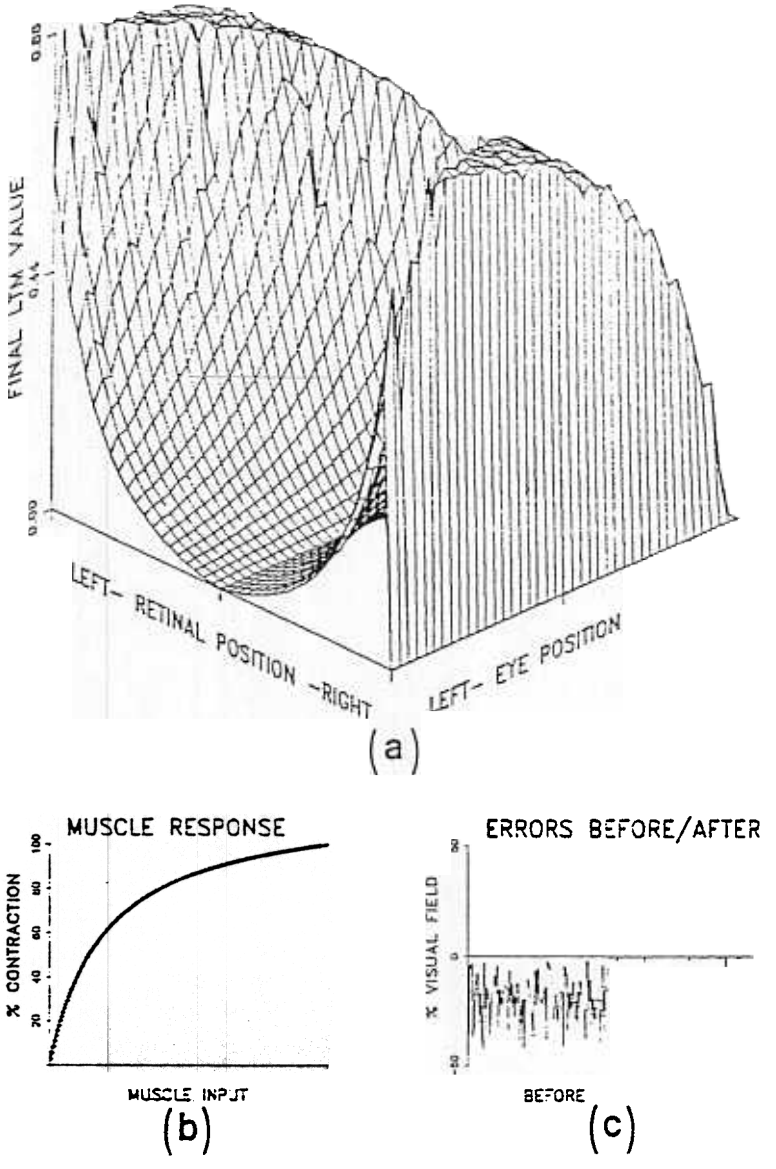

Figure 3.15. Computer simulation of saccadic error correction model with sampling from a non-invariant target position map using a slower-than-linear muscle function and a linear learning function. The following parameters were used in the simulation: $m = 1$, $\alpha = .2$, $\gamma = 1$, $\delta = 1$, $\epsilon = .1$, and $n = 100,000$. (a) Topographic distribution of LTM trace values after learning. (b) Muscle response function used in the simulation. (c) Errors in 100 trials before learning begins and 100 trials after learning ends. Negative values correspond to undershoots and positive values correspond to overshoots.

certain lesions are eventually fully compensated whereas losses after other lesions are at best partially compensated by spared neural subsystems.

An example of how lesions can change learning LTM maps can be developed from the simulation described in Figure 3.16. In this simulation, LTM traces of retinotopic, eye position, and invariant target position sampling maps share the learning load. If the target position map is destroyed, then the remaining retinotopic and eye position LTM traces can absorb the processing load, as in Figure 3.14B. By contrast, if both the target position and the eye position map are destroyed, then the remaining retinotopic LTM traces cannot absorb the full processing load, although they can keep the mean errors centered around the fovea, as in Figure 3.12A. Two sampling maps can be destroyed without preventing full adaptation, if these sampling maps are the retinotopic and the eye position maps. Then the single remaining target position map can absorb the full processing load, as in Figure 3.13.

3.18. Models of Saccadic Error Correction

This section describes the numerical analysis of how 36 network models learn to correct errors of saccadic foveation. The task of the networks is to produce accurate foveations to retinal lights starting from any eye position, even if the muscle plant is nonlinear. The simulations describe learning by one pair of agonist-antagonist muscles. The same mechanism generalizes to any number of independent agonist-antagonist pairs using the sampling anatomy of the AG stage in Figure 3.8.

For definiteness, let the agonist-antagonist muscle pair control horizontal eye movements, and let a one-dimensional strip of cells receive the retinal inputs that drive these muscles. Divide the strip into a right hemifield and a left hemifield. A row of 100 nonfoveal cells form each hemifield in the following simulations. The mechanisms work using any spatial resolution in one and two spatial dimensions.

The simulations are carried out using a discrete time variable as well as a discrete mesh of cells for two reasons: The saccade is a ballistic motion that is initiated by commands set up before it begins, and that is corrected by error signals that are registered after it ends. Use of a continuous time variable can only increase the stability of the computations. This discrete approximation will be refined in Section 3.19. There we will consider effects of inertial properties which develop continuously during a saccade, and will discuss how these tendencies towards dynamic overshoot may be controlled. The results in the present section provide a foundation for these later analyses.

Let the index i, $-100 \leq i \leq 100$, denote the spatial location of a light input on the retina, and the index n, $n \geq 1$, denote the learning trial. A randomly chosen light is assumed to activate the retina, unless the prior saccade was incorrect. In this latter case, the retinal position at which the nonfoveated light is registered after a saccade gets activated on the next trial. This procedure formalizes the idea that a second light position on trial n is the first light position on trial $n + 1$, except when an

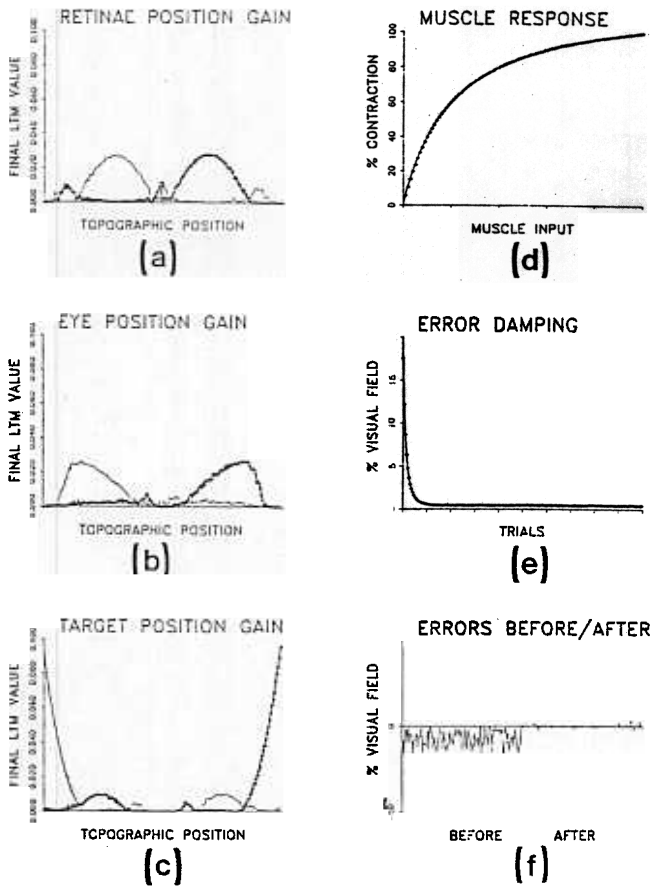

Figure 3.16. Computer simulation of saccadic error correction model with simultaneous sampling from retinal position, invariant target position, and eye position maps using a slower-than-linear muscle function and a linear learning function. The following parameters were used in the simulation: $m = 1$, $\alpha = .2$, $\gamma = 2$, $\delta = 1$, $\epsilon = .01$, and $n = 100,000$. (a), (b), and (c) Topographic distribution of LTM trace values after learning. Bold curves indicate values in the right adaptive gain (AG) hemifields while thin curves indicate values in the left AG hemifields. (d) Slower-than-linear muscle response function used in the simulation. (e) Error damping over 100,000 trials. Error damping value D_n at trial n approximates the average error via the equation $D_{n+1} = (999D_n + \mid E_n \mid)/1000$, where $D_0 = 25$. (f) Errors in 100 trials before learning begins and 100 trials after learning ends. Negative values correspond to undershoots and positive values correspond to overshoots.

accurate foveation occurs. To express this rule formally, let $i = i_n$ be the position of the retinal light on trial n, where $-100 \leq i_n \leq 100$. Position $i_n = 0$ corresponds to a light at the fovea. Let E_n be the second light position that is caused by a saccade to a first light at position i_n. The function E_n also represents the size of the error caused by the nth saccade, since $E_n = 0$ corresponds to a correct saccade. In order to restrict the computation to a discrete array of cells, we also define an error tolerance E, which was chosen equal to .1 in the simulations. In terms of these definitions, let

$$i_{n+1} = \begin{cases} \text{random i}, -100 \leq i \leq 100 \text{ and } i \neq 0 & \text{if } \left| E_n \right| \leq E \\ E_n & \text{if } \left| E_n \right| > E. \end{cases} \tag{3.1}$$

In order to define a complete model, several rules need to be specified.

A. *The Light-Motoneuron Transform*: the rule whereby a light at position $i = i_n$ generates outputs from the motoneurons.

B. *The Motoneuron-Muscle Transform*: the rule whereby outputs from the motoneurons determine prescribed lengths of their target muscles before and after saccades.

C. *The Muscle-Retina Transform*: the rule whereby changes in muscle length cause changes in the position of the light on the retina.

D. *The Retina-Learning Transform*: the rule whereby the new second light position acts as an error signal that alters the sizes of LTM traces at the AG stage.

In order to state these rules clearly, we need to introduce some notation. Since the same Motoneuron-Muscle Transform is used in all models, we start by defining this transform. Let O_{Rn} (O_{Ln}) equal the total motoneuron output to the right (left) muscle after the saccade on trial n, and let M_{Rn} (M_{Ln}) equal the total muscle contraction of the right (left) muscle after the saccade on trial n. In order to relate these two types of functions, we define a *contraction function* $C(w)$ that converts motoneuron signals into muscle contractions. The computation is scaled so that

$$M_{Rn} + M_{Ln} = C(1) \tag{3.2}$$

for all $n \geq 1$. The left and right muscles are assumed to contract and relax in a push-pull fashion.

Motoneuron-Muscle Transform and Push-Pull

Let

$$M_{Rn} = \begin{cases} C(O_{Rn}) & \text{if } i_n > 0 \\ C(1) - C(O_{Ln}) & \text{if } i_n < 0, \end{cases}$$

$$M_{Ln} = \begin{cases} C(1) - C(O_{Rn}) & \text{if } i_n > 0 \\ C(O_{Ln}) & \text{if } i_n < 0, \end{cases}$$

for $n \geq 1$, and

$$M_{RO} = M_{LO} = 1/2C(1). \tag{3.5}$$

Equation (3.3) says that the right muscle contracts if the right hemifield received a light, and relaxes if the left hemifield receives a light. In case $i_n < 0$ of (3.3), O_{Rn} can be defined by the relation

$$O_{Rn} = C^{-1}[C(1) - C(O_{Ln})].$$

Equation (3.4) makes the analogous statements about control of the left muscle. Equation (3.5) says that the eye starts out in a head-in-center position before learning trials begin. Contraction functions of the form

$$C(w) = \frac{w^m}{\alpha^m + w^m}$$

were used in the simulations, where $m = 1$, 2, or 4 and $\alpha = .1$, .2, or .5. Parameter m determines the nature of the muscle plant nonlinearity. The choosing $m = 1$ defines a slower-than-linear nonlinearity. Choosing $m = 2$ or 4 defines an S-shaped, or sigmoidal, nonlinearity. Choice $m = 4$ defines a more nonlinear muscle plant than does choice $m = 2$. Parameter α also controls the nonlinearity of the muscle. A smaller α determines a steeper increase in muscle contraction as a function of w because $C(\alpha) = 1/2$. Different choices of α thus correspond to different thresholds of muscle contraction and different sensitivities of the muscle plant to motoneuron signals. Equation (3.2) shows that the maximal total contraction is scaled to equal $C(1)$, which by (3.7) is less than 1.

We can now define the Muscle-Retina Transform. This amounts to defining the second light position E_n on trial n as a function of the amount of muscle contraction due to the nth saccade. To do so, it is necessary to keep two spatial scales clearly in view. Retinal lights can fall on any position i such that $-100 \leq i \leq 100$, whereas muscles can contract no more than an amount $C(1) < 1$. We assume that the change in retinal position of a fixed light on trial n is proportional to the amount by which the muscles contract or relax on that trial. The proportionality constant need not equal 1 for some of the models to learn accurate foveations. To define E_n, we use the notation

$$[[\xi]] = \begin{cases} \text{largest integer} \leq \xi & \text{if } \xi > 0 \\ \text{smallest integer} \geq \xi & \text{if } \xi \leq 0. \end{cases} \tag{3.8}$$

Muscle-Retina Transform

Let

$$E_n = \begin{cases} \max\{-100, [[i_n + \beta(M_{R,n-1} - M_{Rn})]]\} & \text{if } i_n > 0 \\ \min\{100, [[i_n + \beta(M_{Ln} - M_{L,n-1})]]\} & \text{if } i_n < 0, \end{cases}$$

where

$$\beta = \frac{100\gamma}{C(1)}. \tag{3.10}$$

To understand this definition, consider the case where $i_n > 0$. Then a light hits the right hemifield on trial n. This event causes a saccade towards the right. This saccade cannot move the eye farther than the right muscle can maximally contract. For simplicity, we assume that such a maximal contraction causes the light to fall on the leftmost cell of the array, namely $E_n = -100$. This property explains the use of the function $\max\{-100, \cdot\}$ in this case. All saccadic motions cause the light to excite a definite new cell in the array. This property explains the use of the function $[[\cdot]]$, which causes every motion to excite the cell nearest to the light's new position. Term $i_n + \beta(M_{R,n-1} - M_{Rn})$ says that the new position of the light is determined by the light's initial position i_n plus the amount $\beta(M_{R,n-1} - M_{Rn})$ by which the light moves across the retina. The term $\beta(M_{R,n-1} - M_{Rn})$ says that the amount of retinal motion is proportional to the amount of muscle contraction $M_{Rn} - M_{R,n-1}$ caused by the light. Since the light moves to the left when the right muscle contracts, the change in retinal position is $\beta(M_{R,n-1} - M_{Rn})$ rather than $\beta(M_{Rn} - M_{R,n-1})$. Parameter β in (3.10) scales amount of muscle contraction into amount of retinal motion as follows. By (3.2), term $C(1)$ is the maximal amount of muscle contraction. Dividing $M_{R,n-1} - M_{Rn}$ by $C(1)$ defines a function that stays between -1 and 1. Multiplying this ratio by 100 defines a function that stays between -100 and 100. The extra term γ calibrates the gain of the Muscle-to-Retina Transform. In our simulations, gain values of $\gamma = 1$, 2, or 3 were studied. The equation for saccades to the left in (3.9) (case $i_n < 0$) has a similar interpretation.

We are now ready to define the Retina-Learning Transform. Different learning models use different combinations of sampling maps. Each sampling map sends conditionable signals to the AG stage and then on to the saccade generator (SG) or the motoneuron (MN) stages. To define rules for LTM change, let $z_{Rin}(z_{Lin})$ be the value of the LTM trace from the ith population of a sampling map to the AG strip corresponding to the right (left) muscle at the beginning of trial n. Learning by each LTM trace is assumed to alter the production rate of the chemical transmitter in its synapse (Eccles, 1953; Hebb, 1949; Grossberg, 1968a, 1969b, 1969c; Kandel and Schwartz, 1982). Each LTM trace, in turn, controls the net rate of release of its transmitter in response to its sampling signal. Two types of learning rules have been simulated. In both rules, a *learning function* $L(w)$ converts the position E_n of the light after the nth saccade into the size $L(E_n)$ of a learning signal. We physically interpret $L(E_n)$ as an error signal that is carried by pathways from a retinal map to cerebellar climbing fibers that project to the motor strips of the right and left muscles (Figure 3.8). Since no learning occurs when $E_n = 0$, we choose $L(0) = 0$. Since learning rate should increase, or at least not decrease, as E_n increases, we assumed that $L(w)$ is an increasing function of $w \geq 0$. Since an increase in $z_{Ri,n+1}$ should occur if $E_n > 0$, whereas an increase in $z_{Li,n+1}$ should occur if $E_n < 0$, we assume that $L(w)$ is an odd function of w; viz.,

$$L(w) = -L(-w). \tag{3.11}$$

The two types of learning rules that we have studied can now be stated using the notation $[\xi]^+ = \max(\xi, 0)$.

Hemifield Gradient Learning Rule

Let

$$z_{Ri,n+1} = \delta z_{Rin} + [L(E_n)]^+ \tag{3.12}$$

$$z_{Li,n+1} = \delta z_{Lin} + [-L(E_n)]^+, \tag{3.13}$$

where $0 < \delta \leq 1$.

Fractured Somatotopy Learning Rule

Let

$$z_{Ri,n+1} = [\delta z_{Rin} + L(E_n)]^+ \tag{3.14}$$

and

$$z_{Li,n+1} = [\delta z_{Lin} - L(E_n)]^+, \tag{3.15}$$

where $0 < \delta \leq 1$.

A difference equation such as (3.12) is a discrete approximation to a related differential equation. Rewriting (3.12) as

$$z_{Ri,n+1} - z_{Rin} = -(1 - \delta) z_{Rin} + [L(E_n)]^+, \tag{3.16}$$

the corresponding differential equation is seen to be

$$\frac{d}{dt} z_{Ri} = -(1 - \delta) z_{Ri} + [L(E_n)]^+. \tag{3.17}$$

In (3.17), z_{Ri} is a time average of the error signal $[L(E)]^+$. The averaging rate is $1 - \delta$. If $\delta = 1$, then no forgetting occurs.

The Hemifield Gradient Learning Rule says that at most one of the LTM traces $z_{Ri,n+1}$ and $z_{Li,n+1}$ can grow due to E_n on trial n, since by (3.11), $[L(E_n)]^+ > 0$ only if $E_n > 0$ and $[-L(E_n)]^+ > 0$ only if $E_n < 0$. By contrast, the Fractured Somatotopy Learning Rule says that $z_{Ri,n+1}$ increases by the same amount that $z_{Li,n+1}$ decreases, and conversely, until one of the LTM traces becomes zero. Consequently the sum $z_{Rin} + z_{Lin}$ is constant until one of the LTM traces vanishes.

In the simulations, the learning functions $L(w) = \epsilon w$, $L(w) = \epsilon w^3$, and $L(w) = \{\epsilon$ if $w > 0$, $-\epsilon$ if $w < 0$, and 0 if $w = 0\}$ were used. These choices permitted a comparison of the effects of linear and nonlinear error signals on the learning process. In order to guarantee an incremental effect of error signals on learning and performance, the forgetting rate $1 - \delta$ was chosen small. The values used in the simulations were $\delta = 1$, .999, and .998. We also chose the learning rate ϵ to be larger than the forgetting rate $1 - \delta$. The choices $\epsilon = .002, .005, .01, .1$, and 1 were studied. Too large a choice of ϵ destabilizes the system by amplifying the LTM traces too much on a single trial.

It remains to define the Light-Motoneuron Transform. This transform was chosen differently in different models because the sampling maps that were used vary across models. In every model, prewired light-activated pathways elicit unconditioned saccades even before learning occurs, and competition occurs between agonist-antagonist muscle commands (Section 3.7). The agonist-antagonist competition can occur at any of several anatomical stages. If the Fractured Somatotopy Learning Rule (3.14)-(3.15) holds, then competition between agonist-antagonist LTM traces already occurs within the AG stage. A subsequent stage of competition is nonetheless still necessary to guarantee the push-pull Motoneuron-Muscle Transform (3.3)-(3.4). If both the left and the right saccade generators receive positive signals from the AG stage, then their outputs must compete before the muscles receive the net signal, so that the motoneurons whose SG has the larger output will receive a positive signal, and the other motoneurons will receive a negative signal, thereby realizing push-pull. In such a network, two agonist-antagonist competition stages occur: intracerebellar competition and competition at a stage between the SG and the MN stages. In an alternative scheme to achieve muscle push-pull, right and left hemifield outputs from the AG stage compete after the AG stage but before the SG stage. Then only one SG can generate an output signal. This output signal must then excite its own motoneurons and inhibit the antagonist motoneurons to achieve push-pull. In this network, there are three, rather than two, agonist-antagonist competition stages: intracerebellar, pre-SG, and post-SG competition.

If the Hemifield Gradient Learning Rule (3.12)-(3.13) is used, then agonist-antagonist competition must occur at some post-SG stage to realize LTM competition, as well as push-pull competition.. The pre-SG and post-SG competitive anatomies described above achieve these properties with this learning rule. For definiteness, we write down only equations for the pre-SG competitive anatomy. Post-SG competition gives rise to similar learning properties, but the push-pull equations (3.3)-(3.4) must then be redefined in an obvious way.

The input to the motoneurons in all the simulations is a sum of an unconditioned retinotopic signal plus conditionable signals from one or more sampling maps. The unconditioned signal U_{Rin} (U_{Lin}) from retinotopic cell i to the right (left) MN at the end of trial n is

$$U_{Rin} = S_{in}^{(r)} G_{Ri} \tag{3.18}$$

and

$$U_{Lin} = S_{in}^{(r)} G_{Li}. \tag{3.19}$$

Term $S_{in}^{(r)}$ is the signal emitted by the ith retinotopic cell, and G_{Ri} (G_{Li}) is the path strength of the ith pathway to the right (left) MN. For simplicity, let

$$S_{in}^{(r)} = \begin{cases} 1 & \text{if } i = i_n, \\ 0 & \text{otherwise,} \end{cases} \tag{3.20}$$

where i_n is defined by (3.1). In a similar fashion, sampling signals will be chosen equal to 1 or 0 depending upon whether or not the corresponding sampling map population is activated on a given trial. The definitions of the *spatial gradient functions* G_{Ri} and G_{Li} embody the intuition that prewired connections tend to cause larger contractions in response to more eccentric retinal inputs (Figure 2.1). The networks can learn to foveate in response to a wide variety of such spatial gradient functions G_{Ri} and G_{Li}. For definiteness, we let the strength of these gradient connections increase as a linear function of retinal eccentricity; namely,

$$G_{Ri} = G[i]^+ \tag{3.21}$$

and

$$G_{Li} = G[-i]^+. \tag{3.22}$$

In the simulations described in Figures 3.11-3.15, we chose $G = .1$. Other things being equal, smaller G values induce learning of larger LTM traces at the AG stage.

We can now define the combined effects of unconditioned and conditioned movement signals on the Light-Motoneuron Transform given different combinations of sampling maps.

A. Purely Retinotopic Sampling

In order to describe the motoneuron outputs O_{Rn} and O_{Ln} that correspond to a retinotopic sampling map, we use a superscript "(r)", as in the notations $S_{in}^{(r)}$ and $z_{Rin}^{(r)}$ for sampling signals and LTM traces, respectively. The total output signal from the right MN stage after the nth saccade terminates is defined to be

$$O_{Rn} = \max\{1, [\sum_{i \in R} S_{in}^{(r)}(z_{Rin}^{(r)} - z_{Lin}^{(r)}) + \sum_{i \in R} P_{Rin} + O_{R,n-1}]^+\}. \tag{3.23}$$

The expression $\max\{1, \cdot\}$ in (3.23) says that the right muscle contracts maximally when it receives a unit signal, as in (3.2). This expression, which forms part of all subsequent O_{Rn} and O_{Ln} equations, will henceforth be omitted for notational convenience.

The sums $\sum_{i \in R}$ in (3.23) are taken over all cells in the retinotopic sampling map. Since on trial n, the active sampling position is $i = i_n$, (3.20) implies that all terms in the sum vanish except term $i = i_n$. Thus (3.23) simplifies to

$$O_{Rn} = [S_{i_n n}^{(r)}(z_{Ri_n n}^{(r)} - z_{Li_n n}^{(r)}) + S_{i_n n}^{(r)} G[i_n]^+ + O_{R,n-1}]^+. \tag{3.24}$$

In (3.24), term $S_{i_n n}^{(r)} z_{Ri_n n}^{(r)}$ says that the (i_n)th retinotopic population reads out a movement signal from the AG motor strip corresponding to the right muscle R. This signal is the product of the retinotopic sampling signal $S_{i_n n}^{(r)}$

times the LTM trace $z^{(r)}_{Ri_n n}$ from retinotopic position i_n to muscle strip R. Due to the multiplicative form of this relationship, we say that the LTM trace *gates* the sampling signal. Term $-S^{(r)}_{i_n n} z^{(r)}_{Li_n n}$ says that a similar LTM-gated read-out occurs from the AG strip corresponding to the left muscle strip L. Due to the minus sign in front of this expression, the left-muscle signal competes with the right-muscle signal before the net signal can reach the right MN. Term $S^{(r)}_{i_n n} G[i_n]^+$ says that an unconditioned movement signal is also read-out by the (i_n)th retinotopic signal. The total, unconditioned plus conditioned, signal adds onto the previous MN activity $O_{R,n-1}$. If the updated total activity is positive, then the $[\cdots]^+$ enables a signal to be emitted to the right muscle.

Equation (3.24) can be further simplified. Using (3.20) again, we can write

$$O_{Rn} = [z^{(r)}_{Ri_n n} - z^{(r)}_{Li_n n} + G[i_n]^+ + O_{R,n-1}]^+. \tag{3.25}$$

The subscripts in this formula are unwieldly. Henceforth we write subscripts i instead of i_n to simplify the notation. Then (3.25) becomes

$$O_{Rn} = [z^{(r)}_{Rin} - z^{(r)}_{Lin} + G[i_n]^+ + O_{R,n-1}]^+. \tag{3.26}$$

A similar analysis shows that

$$O_{Ln} = [z^{(r)}_{Lin} - z^{(r)}_{Rin} + G[-i_n]^+ + O_{L,n-1}]^+. \tag{3.27}$$

B. Invariant Target Position Map

Using the same simplified notation as in (3.27), we can recursively define the motoneuron output corresponding to the right muscle by

$$O_{Rn} = [z^{(t)}_{Rkn} - z^{(t)}_{Lkn} + G[i_n]^+ + O_{R,n-1}]^+, \tag{3.28}$$

where $z^{(t)}_{Rkn}$ and $z^{(t)}_{Lkn}$ are the target position map LTM traces. In (3.28), the target position on the kth trial is denoted by $k = k_n$. It is necessary to define k_n in terms of the retinotopic position i_n and the initial eye position j_n at the beginning of trial n. We find that

$$k_n = \begin{cases} i_n + i_j & \text{if } -100 \leq i_n + j_n \leq 100 \\ \text{undefined} & \text{if } |\, i_n + j_n \,| > 100 \end{cases} \tag{3.29}$$

and

$$j_n = \begin{cases} \beta M_{R,n-1} & \text{if } i_n > 0 \text{ and } \beta M_{R,n-1} \leq 100 \\ \beta M_{L,n-1} & \text{if } i_n < 0 \text{ and } \beta M_{L,n-1} \geq -100 \\ \text{undefined otherwise.} \end{cases} \tag{3.30}$$

Function j_n in (3.30) defines the initial eye position at the beginning of trial n, in terms of the amount of muscle interaction in (3.3) and (3.4) due to the previous saccade. Then function k_n in (3.29) determines the target position arising from retinotopic position i_n and initial eye position j_n. In cases when k_n is undefined, the next retinotopic position i_{n+1} is chosen randomly. In a similar fashion, the motoneuron output corresponding to the left muscle is defined by

$$O_{Ln} = [z_{Lkn}^{(t)} - z_{Rkn}^{(t)} + G[-i_n]^+ + O_{L,n-1}]^+. \tag{3.31}$$

Two other combinations of sampling maps can be defined by using these definitions.

C. Invariant Target Position Map Plus Retinotopic Map

Let

$$O_{Rn} = [(z_{Rkn}^{(t)} - z_{Lkn}^{(t)}) + (z_{Rin}^{(r)} - z_{Lin}^{(r)}) + G[i_n]^+ + O_{R,n-1}]^+ \tag{3.32}$$

d

$$O_{Ln} = [(z_{Lkn}^{(t)} - z_{Rkn}^{(t)}) + (z_{Lin}^{(r)} - z_{Rin}^{(r)}) + G[-i_n]^+ + O_{L,n-1}]^+. \tag{3.33}$$

D. Retinotopic Map Plus Eye Position Map

Let

$$O_{Rn} = [(z_{Rin}^{(r)} - z_{Lin}^{(r)}) + (z_{Rjn}^{(p)} - z_{Ljn}^{(p)}) + G[i_n]^+ + O_{R,n-1}]^+ \tag{3.34}$$

$$O_{Ln} = [(z_{Lin}^{(r)} - z_{Rin}^{(r)}) + (z_{Ljn}^{(p)} - z_{Rjn}^{(p)}) + G[-i_n]^+ + O_{L,n-1}]^+. \tag{3.35}$$

In (3.34) and (3.35), $z_{Rjn}^{(p)}$ and $z_{Ljn}^{(p)}$ are the eye position map LTM traces. The subscript $j = j_n$ is defined by (3.30).

E. Noninvariant Target Position Map

A similar definition of MN output signal can be given for the case wherein each pair (i, j) of retinotopic positions and initial eye positions activates its own sampling map population. Essentially perfect learning can rapidly occur in this case even if no LTM agonist-antagonist competition occurs. This is due to the fact that each (i, j) pair controls an LTM trace z_{ij} that is unique to its position. For example, the learning simulation described in Figure 3.15 used the MN signals

$$O_{Rn} = [z_{ijn} + G[i_n]^+ + O_{R,n-1}]^+ \tag{3.36}$$

$$O_{Ln} = [z_{ijn} + G[-i_n]^+ + O_{L,n-1}]^+ \tag{3.37}$$

where

$$z_{ij,n+1} = [z_{ijn} + L(E_n)]^+. \tag{3.38}$$

In these simulations, $1 \leq i, j \leq 40$, thereby generating 1600 sampling populations.

F. Retinotopic Map Plus Initial Eye Position Map Plus Invariant Target Position Map

Let

$$\begin{aligned} O_{Rn} = [(z_{Rin}^{(r)} - z_{Lin}^{(r)}) + (z_{Rjn}^{(p)} - z_{Ljn}^{(p)}) \\ + (z_{Rkn}^{(t)} - z_{Lkn}^{(t)}) + G[i_n]^+ + O_{R,n-1}]^+ \end{aligned} \tag{3.39}$$

and

$$\begin{aligned} O_{Ln} = [(z_{Lin}^{(r)} - z_{Rin}^{(r)}) + (z_{Ljn}^{(p)} - z_{Rjn}^{(p)}) \\ + (z_{Lkn}^{(t)} - z_{Rkn}^{(t)}) + G[-i_n]^+ + O_{L,n-1}]^+ \end{aligned} . \tag{3.40}$$

The formal lesions describes in Section 3.17 can be carried out on equations (3.39) and (3.40) by deleting the LTM traces with superscripts (t), then (t) and (p), and then (r) and (p).

3.19. Dynamic Coasting

In the preceding sections, we have analysed examples in which the final position of the eye is a function $C(O_{Rn})$ or $C(O_{Ln})$ of the total movement signals O_{Rn} and O_{Ln} to an agonist-antagonist pair of eye muscles. *In vivo*, the eye may continue moving for awhile after the saccade generator shuts off. Van Gisbergen, Robinson, and Gielen (1981) have noted that "after the main pulse the eye requires time to coast to a stop" (p.427). The duration of an agonist saccadic command may be "only 82.2% of saccade duration on the average, indicating that the saccade does outlast [the agonist command] by about 18%" (p.427).

Dynamic coasting is due to the fact that the eyeball builds up inertia during the saccade. This inertia enables the eyeball to keep moving after the saccadic command terminates. Dynamic coasting does not imply that the saccade must overshoot its target. Indeed, second light error signals are registered only after a saccade terminates, and are indifferent to whether or not part of the saccade was due to eyeball inertia.

On the other hand, the question remains concerning what types of sampling maps can use second light error signals to generate accurate saccades even if these saccades include an interval of dynamic coasting. A deeper question must also be considered: Why are not the adaptive gain mechanisms of the saccadic movement system sufficient to compensate for dynamic coasting? Why cannot these adaptive mechanisms terminate a saccade more quickly after the saccade generator shuts off?

We will suggest a simple, albeit tentative, answer to both questions. This answer is consistent with the computer simulations that are summarized in the preceding and ensuing sections. A more complete answer must await an analysis of how the AG stage controls a complete mechanical model of an eyeball and its extraocular muscles.

3.20. Outflow-Inflow Comparisons: A Large Movement as a Series of Small Movement Segments

In Section 1.10, we noted that comparisons between outflow signals and inflow signals are used to linearize the response of the muscle plant to outflow movement signals. This mechanism enables the brain to use outflow-generated corollary discharges as a measure of eye position, since the actual eye position will then tend to covary with the size of the outflow signals. This mechanism works by letting mismatches of outflow and inflow signals generate error signals that can change the size of the total outflow signal to the muscle plant. The conditioned part of the outflow signal adds or subtracts the correct amount to make the muscle react approximately linearly to the total outflow signal. In effect, this conditioned signal automatically changes the gain of the total outflow signal through learning.

In Chapter 5, this linearization mechanism will be described in detail. We will argue that matches and mismatches between outflow and inflow are registered throughout a saccade. The gain of the movement command can hereby be learned and updated sequentially as a saccade proceeds. We suggest that its takes anywhere from 10–20 msec for this learning circuit to encode an outflow-inflow mismatch, register it as a error signal, and then reset the circuit to encode the next possible mismatch. In this way. the circuit breaks up a total movement into small movement segments. The circuit learns and reads-out a temporal series of gains, each one of which is capable of approximately linearizing one segment of the total movement.

3.21. Mismatch due to Plant Nonlinearity or to Dynamic Coasting?

The outflow-inflow interface, or OII, at which mismatches are registered cannot distinguish between mismatches due to plant nonlinearity and mismatches due to dynamic coasting. The question thus arises: If the OII can linearize the muscle response, then why cannot the OII prevent dynamic coasting? We suggest that the OII performs both tasks equally well, but that the 10–20 msec delay in the learning circuit enables a certain amount of nonlinear muscle response *and* of dynamic coasting to occur.

In particular, the conditioned gain corresponding to a particular eye position tends to be an average of all the gains that are appropriate for saccades passing through that position. This average gain will tend to be smaller than the gain needed to prevent coasting during saccades which reach their maximal velocity through that position. Hence some coasting must be expected. This argument suggests that the amount of coasting

should increase with the cycle time of the learning circuit. The amount of coasting should also increase if the average speed of saccades passing through prescribed eye positions is much less than the speed required by a suddenly imposed experimental manipulation.

3.22. Adaptive Control of Dynamic Coasting

Given that some dynamic coasting is to be expected, it remains to explain how accurate foveations can nonetheless be learned. In the following analysis, we consider several approximate rules to express the effects of dynamic coasting, and describe computer simulations which demonstrate how well the resultant network learns to foveate.

First, we need a rule to replace equations (3.3) and (3.4). To replace (3.3), we considered the following rule.

Dynamic Coasting Rule

$$M_{Rn} = \begin{cases} C(O_{Rn}) + D(C(O_{Rn}) - M_{R,n-1}) & \text{if } i_n > 0 \\ C(1) - C(O_{Ln}) & \text{if } i_n < 0. \end{cases} \tag{3.41}$$

A similar rule is defined for M_{Ln}. Equation (3.41) differs from (3.3) by the term

$$D(C(O_{Rn}) - M_{R,n-1}), \tag{3.42}$$

where $D(\xi)$ may be a linear or nonlinear function of the difference $\xi = C(O_{Rn}) - M_{R,n-1}$. This term expresses the amount of coasting that occurs over and beyond the movement due directly to the saccadic command $C(O_{Rn})$. Term (3.42) makes rigorous the hypothesis that the amount of coasting increases as a function of how much the new saccadic command $C(O_{Rn})$ exceeds the previous eye position, as expressed by $M_{R,n-1}$. In other words, more coasting can occur if the eye movement is bigger, other things being equal.

It is also necessary to consider more sophisticated rules for O_{Rn} and O_{Ln}. Consider, for example, the old rule (3.34) for combining a retinotopic sampling map with an eye position sampling map; namely, the

Static Command Rule

$$O_{Rn} = [S_n + O_{R,n-1}]^+, \tag{3.43}$$

where

$$S_n = (z_{Rin}^{(r)} - z_{Lin}^{(r)}) + (z_{Rjn}^{(p)} - z_{Ljn}^{(p)}) + G[i_n]^+. \tag{3.44}$$

This rule does not provide an adequate summary of the total output signal in situations where part of this signal may be due to a conditioned gain that is sensitive to the amount of dynamic coasting. In order to partially overcome this deficiency, we compared computer simulations using (3.43) with computer simulations using the

Dynamic Command Rule

$$O_{Rn} = \left[S_n + C^{-1}(M_{R,n-1})\right]^+. \tag{3.45}$$

Rule (3.45) acknowledges that the initial position $C^{-1}(M_{R,n-1})$ of the eye before the nth saccade begins may be due to the combined effects of the saccade command $C(O_{R,n-1})$ and of the dynamic coast $D(C(O_{R,n-1}) - M_{R,n-1})$ in (3.41). Rules (3.43) and (3.45) are identical in cases where no dynamic coasting occurs, since then $M_{R,n-1} = C(O_{R,n-1})$. The present discussion thus generalizes the analysis of Section 3.19 to the case where dynamic coasting can occur.

In the computer simulation summarized by Figure 3.17, we chose a linear dynamic coast function

$$D(\xi) = \frac{\xi}{C(1)} \tag{3.46}$$

and the static command rule (3.43). Despite the linearity of $D(\xi)$, the system's ability to learn accurate foveations deteriorated relative to the situation depicted in Figure 3.14. By contrast, in Figure 3.18, the same linear dynamic coast function (3.46) was paired with the dynamic command rule (3.45). Learning significantly improved.

In Figure 3.18, a nonlinear dynamic coast function

$$D(\xi) = C(\frac{\xi}{C(1)}) \tag{3.47}$$

was used where, as in all these simulations,

$$C(w) = \frac{w}{.2 + w}. \tag{3.48}$$

When this slower-than-linear signal function was paired with the static command rule (3.43), an even more serious breakdown of saccadic learning occurred. In Figure 3.20, by contrast, (3.47) was paired with the dynamic command rule (3.45), and learning was again greatly improved.

Figures 3.21 and 3.22 show that a change of the nonlinearity which defines the dynamic coast function can alter the details of learning, but not the qualitative conclusion drawn from Figures 3.19 and 3.20. In both Figure 3.21 and 3.22, we chose

$$D(w) = \frac{(\frac{w}{C(1)})^2}{.2^2 + (\frac{w}{C(1)})^2} \tag{3.49}$$

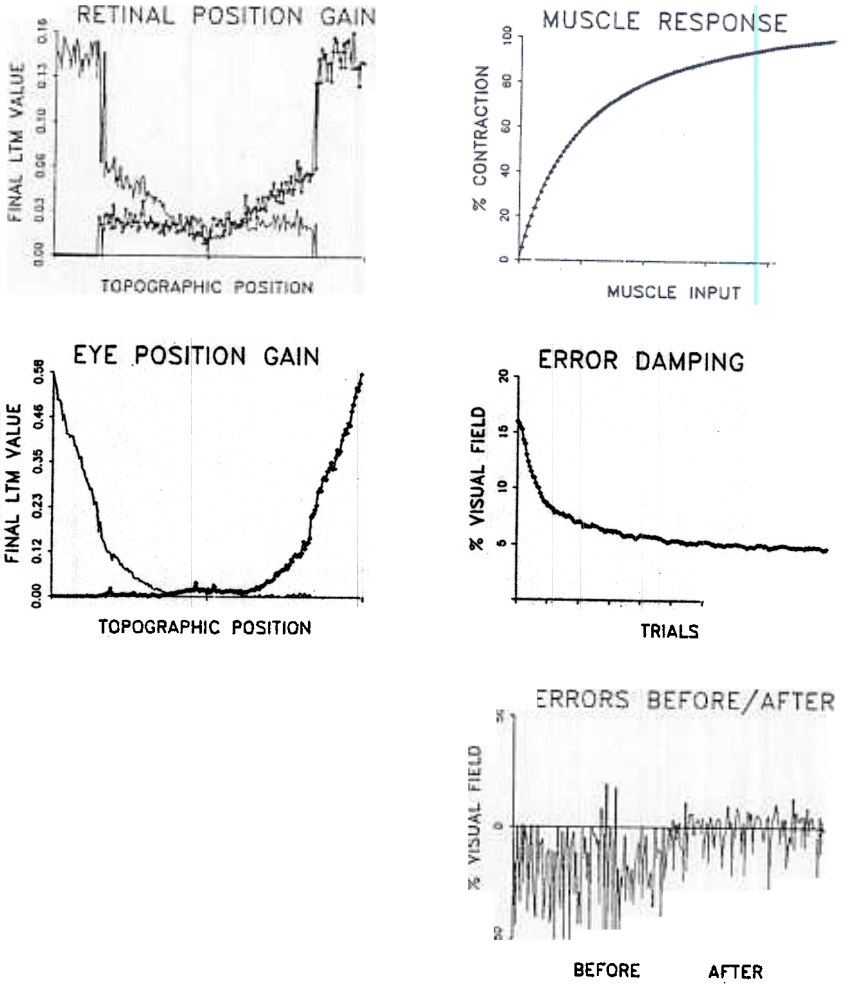

Figure 3.17. Computer simulation of learning using a linear dynamic coast function, a static command rule, and a slower-than-linear muscle response. See text for details.

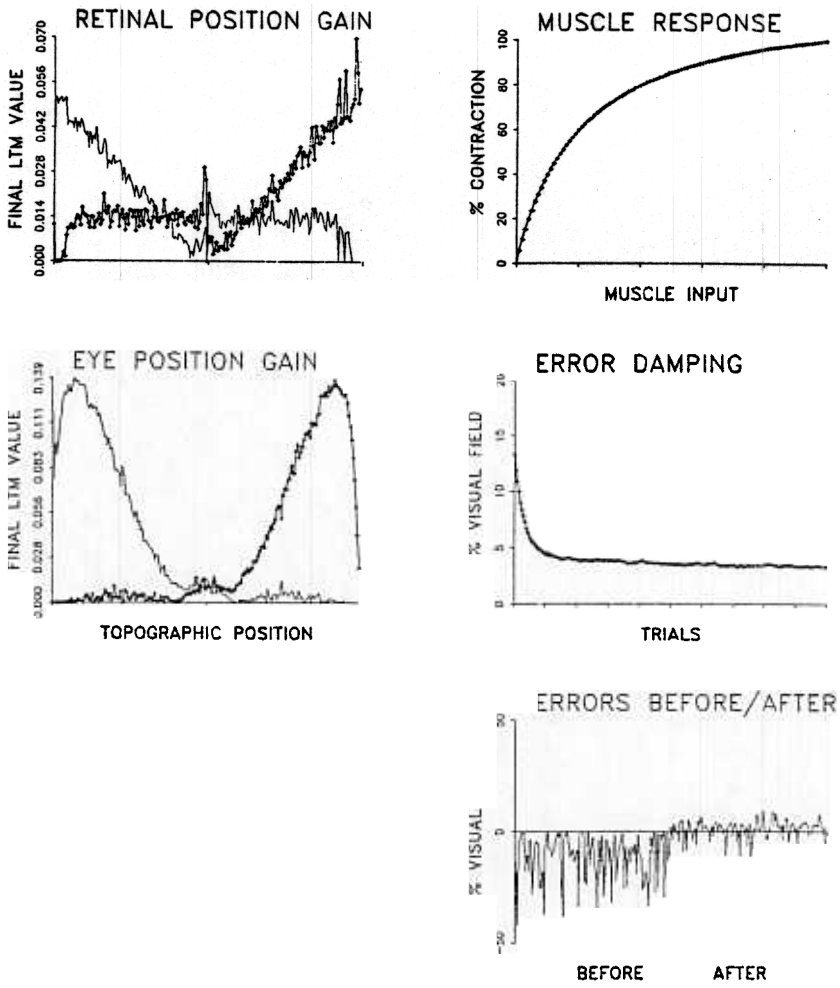

Figure 3.18. Computer simulation of learning using a linear dynamic coast function, a dynamic command rule, and a slower-than-linear muscle response. Learning is much better than in Figure 3.17.

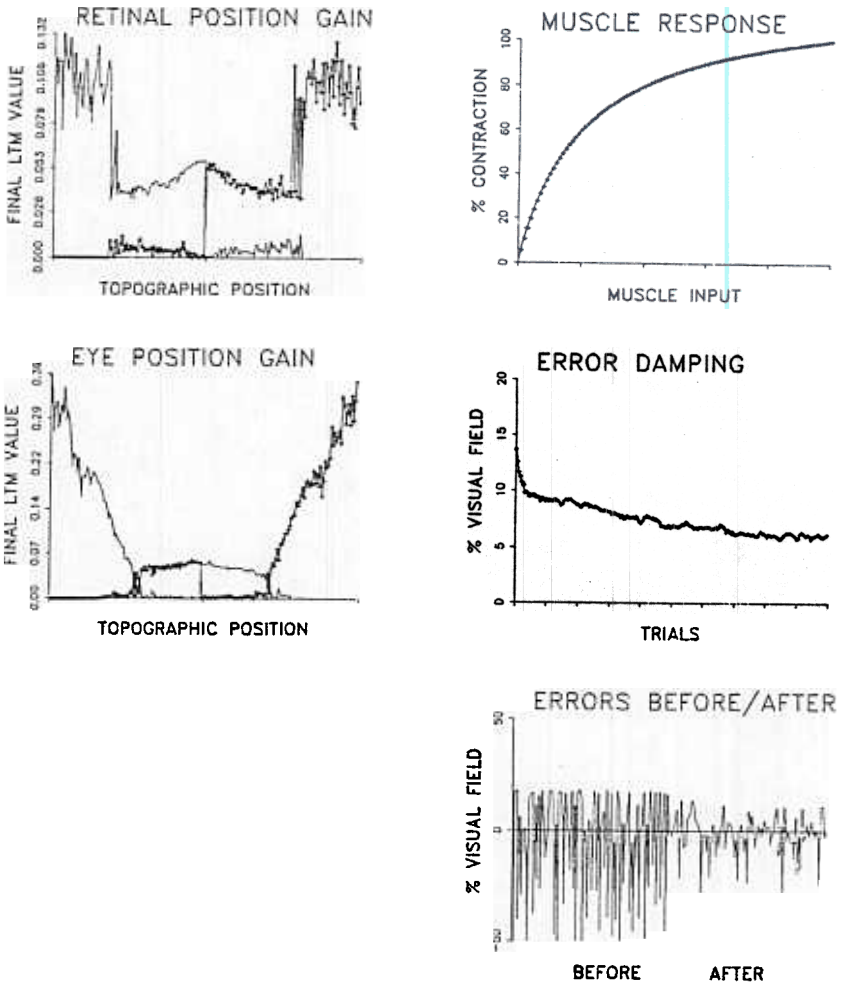

Figure 3.19. Computer simulation of learning using a slower-than-linear dynamic coast function, a static command rule, and a slower-than-linear muscle response.

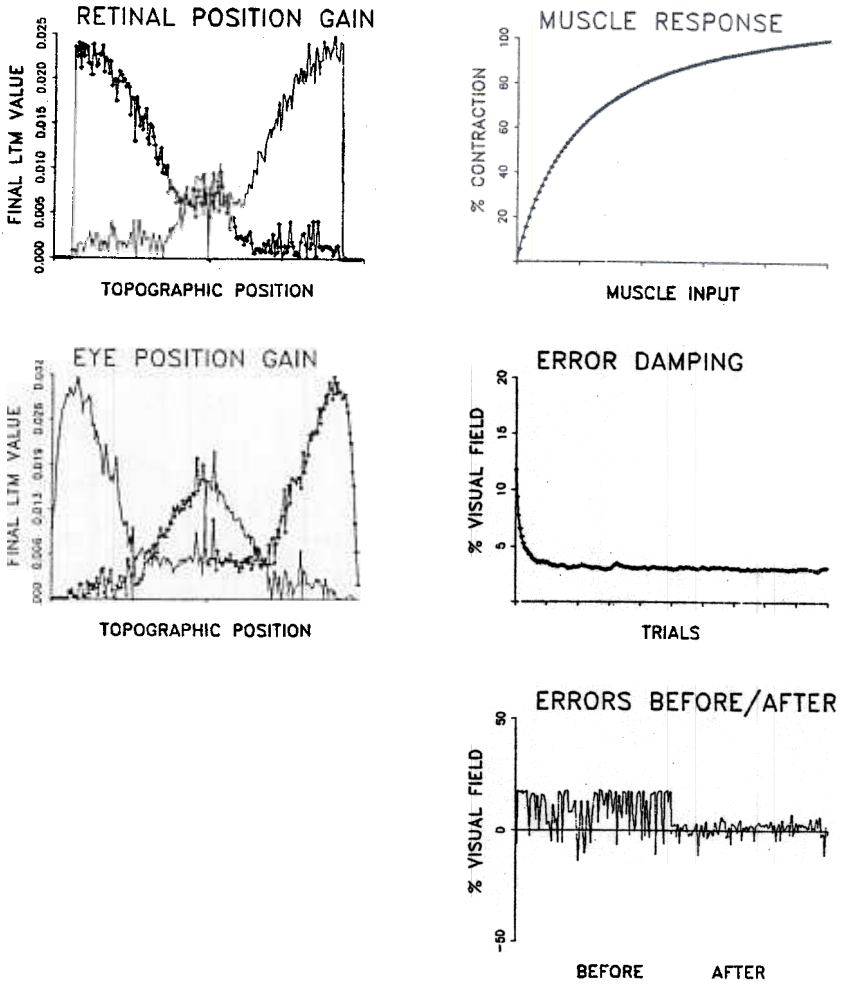

Figure 3.20. Computer simulation of learning with a slower-than-linear coast function, a dynamic command rule, and a slower-than-linear muscle response. Learning is much better than in Figure 3.19.

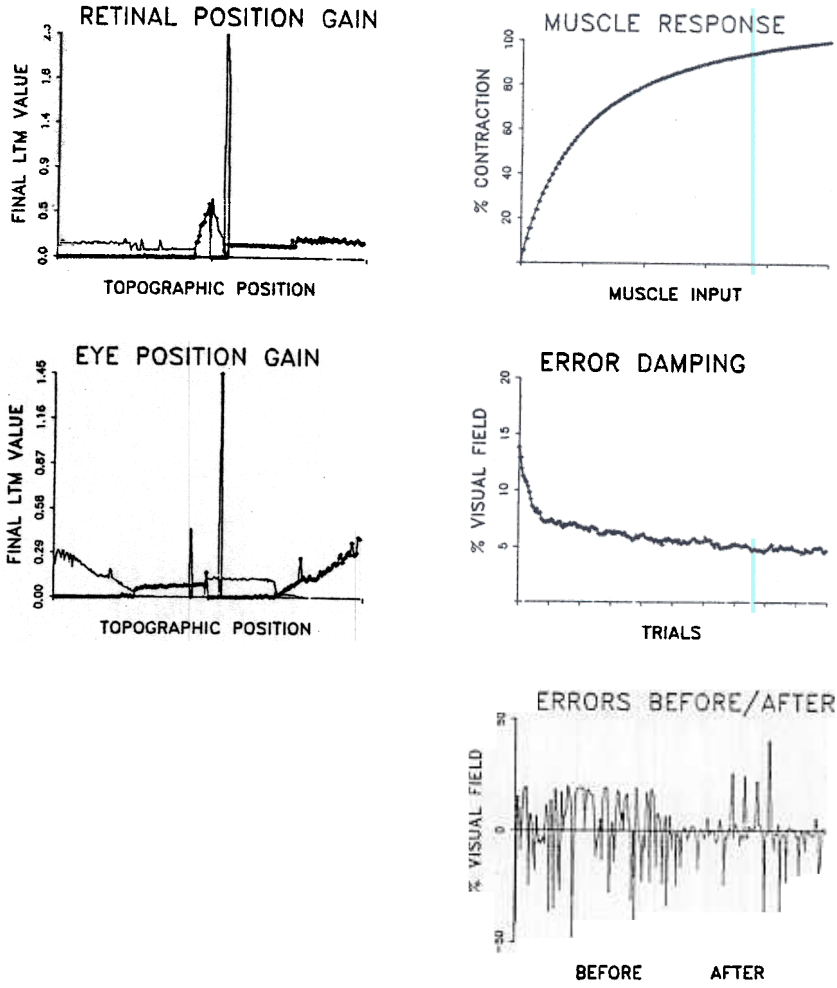

Figure 3.21. Computer simulation of a sigmoid coast function, a static command rule, and a slower-than-linear muscle response.

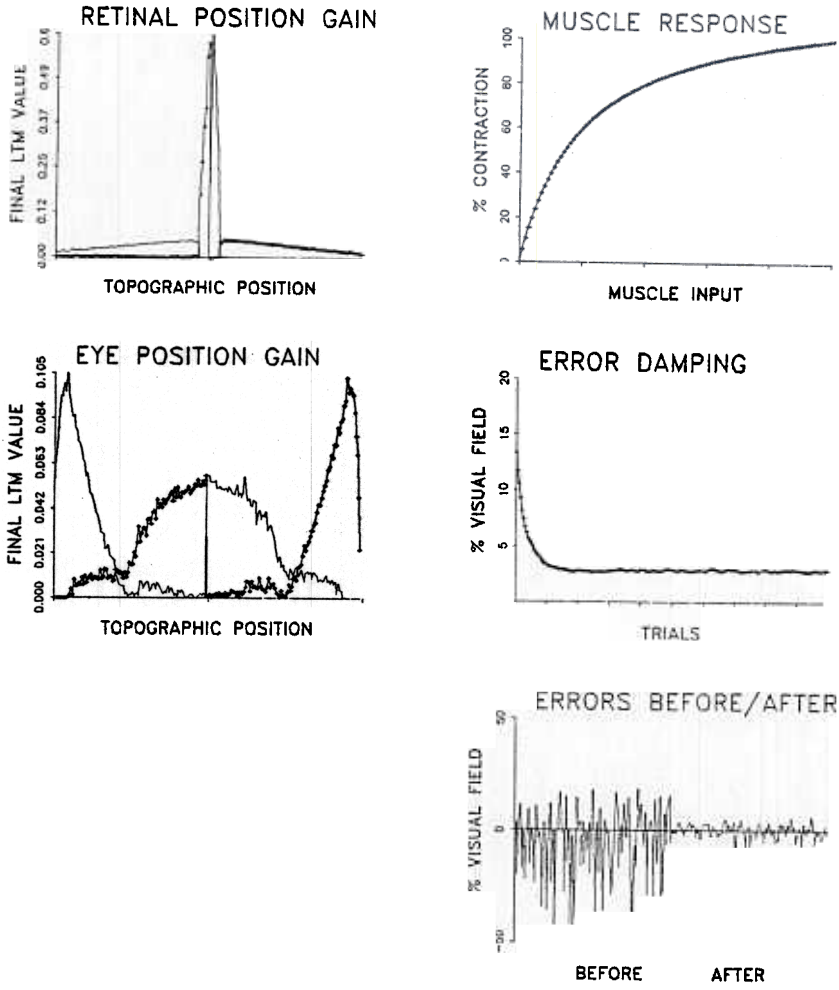

Figure 3.22. Computer simulation of a sigmoid coast function, a dynamic command rule, and a slower-than-linear muscle response. Learning is much better than in Figure 3.21.

instead of (3.47). Function $D(w)$ in (3.49) is a sigmoidal signal function which is quadratically nonlinear at the small w values where (3.47) is approximately linear. When paired with a static command rule in Figure 3.21, poor learning again occurred. When paired with a dynamic command rule in Figure 3.22, excellent learning again occurred.

It remains to physically interpret term $C^{-1}(M_{R,n-1})$ in the dynamic command rule (3.45). Until a complete eyeball and muscle plant is simulated, our interpretation of this term must be cautious. The critical issue is: What circuit can realize commands such as $C^{-1}(M_{R,n-1})$ during the nth saccade? The most likely possibility is the circuit which linearizes the muscle plant. If this interpretation is correct, then (3.45) is just a discrete approximation to the dynamic process whereby the muscle linearization circuit updates movement segments in a somewhat loose but effective fashion, at least from the viewpoint of enabling accurate foveations to be learned.